Preprint
Riedesel, S., Jain, M., submitted. Excited state lifetime of electron trapping centres in alkali feldspars.
The manuscript has been submitted to Radiation Measurements.

This is a **preprint** and has **not been peer-reviewed.**

The article has been submitted for peer-review to *Radiation Measurements* as:

Riedesel, S., Jain, M., submitted. Excited state lifetime of electron trapping centres in alkali feldspars. Radiation Measurements.

Excited state lifetime of electron trapping centres in alkali feldspars

Svenja Riedesel[a,b] and Mayank Jain[a]

[a] Radiation Physics Division, Department of Physics, Technical University of Denmark, Risø Campus, Roskilde, Denmark

[b] Institute of Geography, University of Cologne, Cologne, Germany

Preprint
Riedesel, S., Jain, M., submitted. Excited state lifetime of electron trapping centres in alkali feldspars.
The manuscript has been submitted to Radiation Measurements.

Excited state lifetime of electron trapping centres in alkali feldspars

Svenja Riedesel[a,b] and Mayank Jain[a]

[a] Radiation Physics Division, Department of Physics, Technical University of Denmark, Risø Campus, Roskilde, Denmark

[b] Institute of Geography, University of Cologne, Cologne, Germany

Abstract

The development of the infrared stimulated luminescence (IRPL) signal enables the direct non-destructive probing of the trapped electron population in feldspars. Whilst IRPL offers great perspectives for luminescence dating, it also enables detailed, site-selective measurements of the defects emitting IRPL at 880 nm ($IRPL_{880}$) and 955 nm ($IRPL_{955}$), allowing us to advance our understanding of the defects participating in luminescence production in feldspars.

Here we performed time-resolved IRPL measurements to investigate the excited state lifetimes of $IRPL_{880}$ and $IRPL_{955}$ electron trapping centres of chemically and structurally different feldspars. Our measurements reveal a three component off-time decay for the $IRPL_{880}$ and $IRPL_{955}$ signals. The fastest lifetime (τ_1) fitted to the $IRPL_{880}$ data is consistent with the switch off time of the 830 nm excitation laser; therefore, we cannot conclude whether such a short lifetime component is indeed present in the signal. The two slower lifetimes (τ_2 and τ_3) dominate the $IRPL_{880}$ and $IRPL_{955}$ signals and thus give information on excited state lifetimes in the electron trapping centres investigated. When comparing the chemically and structurally different alkali feldspars, we observed τ_2 lifetimes ranging from 2 µs to 6 µs in case of $IRPL_{880}$ and from 2 µs to 7 µs for $IRPL_{955}$. In case of τ_3 we observed lifetimes from 7 µs to 25 µs for $IRPL_{880}$ and lifetimes from 8 µs to 22 µs for $IRPL_{955}$. Overall, we observe a slight decreasing trend in τ_3 lifetime with decreasing K-feldspar content. Thermal depletion of the trapped electron population results in different behaviour for τ_2 and τ_3 lifetimes: While τ_2 lifetimes decrease with increasing preheat temperature, τ_3 lifetimes are found to be independent of the size of the trapped charge population.

Our data shows that the lifetimes not only reflect excited to ground state relaxation, but that they are also affected by alternative detrapping or recombination routes from the excited state.

Keywords

Feldspars, photoluminescence, time-resolved luminescence, IRPL, lifetime

1 Introduction

Feldspars are wide band gap materials with the ability to trap and store charge within defects in their crystal lattice, enabling the use of feldspars as natural dosimeters to constrain depositional histories in archaeological and geological contexts. The charge storage ability of feldspars is affected by athermal signal loss, termed fading (Wintle, 1973; Visocekas, 1985), which, unless corrected for, leads to age underestimation (Huntley and Lamothe, 2001; Kars et al., 2008). However, over the past one and a half decades advances in feldspar luminescence have helped to minimise the impact of fading on the luminescence results (cf. Thomsen et al., 2008; Thiel et al., 2011; Li and Li, 2011; Prasad et al., 2017). One of these advances is the development of infrared photoluminescence (IRPL; Prasad et al., 2017). IRPL not only lowers fading compared to conventional, recombination-based luminescence techniques (Kumar et al., 2020), such as infrared stimulated luminescence (IRSL; Hütt et al., 1988), it also enables the non-destructive probing of trapped electrons within electron trapping centres in the feldspar lattice (Prasad et al., 2017).

Excitation spectra of feldspars reveal a strong resonance peak in the infrared (~1.45 eV; Hütt et al., 1988, Kars et al., 2013, Riedesel et al., 2018). Stimulating irradiated feldspars with IR photons, causes excitation of electrons from the ground state of the electron trapping centres to the excited state. Radiative excited state to ground state transition within the electron trapping centres results in the emission of IR photons with energies of 1.3 eV (~955 nm) and 1.41 eV (~880 nm). These two main IRPL emissions, henceforth termed $IRPL_{880}$ and $IRPL_{955}$, have been detected in feldspars and have been associated with two different defect sites in the crystal (Kumar et al. 2018; Jain et al., 2020; Riedesel et al., 2021a). However, the crystal defects functioning as electron trapping centres in feldspars are yet to be identified. Time-resolved luminescence techniques allow the measurement of excited to ground state relaxation times within a defect and thus help to improve our understanding the type of defect and transition (i.e. allowed or spin-forbidden) involved in the luminescence process.

Conventional luminescence measurements utilise continuous wave (CW) stimulation. In these CW luminescence measurements, sample material is stimulated using LEDs or laser diodes for a given amount of time, usually tens to hundreds of seconds. During these CW stimulations, the sample's (anti-Stokes) emission is recorded by a photomultiplier (PMT), or by a (electron multiplying) charge coupled device ((EM)-CCD). In contrast, during time-resolved measurements the excitation light source is pulsed on and off and the emission is recorded during on- and off-times. In many cases, also in the present study, the emitted photons are detected using time-correlated single-photon counting (TCSPC; Lapp et al., 2009). TCSPC allows recording the arrival time of each photon at the detector. Summing the luminescence response of several thousand pulses results in the photon arrival time distribution,

which can then be used for fitting the off-time decay to obtain lifetimes of the excited state of the defect probed during the measurement.

Time-resolved luminescence measurements of feldspars have been performed previously. Most of these focussed on characterising feldspar IRSL emissions in the UV, blue, yellow-green and red, in order to understand the defects and transitions involved in electron-hole recombination processes in feldspars (e.g. Sanderson and Clark, 1994; Clark et al., 1997; Clark and Bailiff, 1998; Tsukamoto et al., 2006; Ankjærgaard and Jain, 2010; Jain and Ankjærgaard, 2011; Pagonis et al., 2012; Riedesel et al., 2023). Whilst considerable effort has been put into understanding the luminescence centres probed by electron-hole recombination in feldspars and their resulting luminescence, only very little is known about the lifetimes of internal transitions within the electron trapping centres in feldspars. Prasad et al. (2017) investigated three different feldspar samples and measured the off-time $IRPL_{955}$ emission at room temperature (295 K) and at 7 K. They found that it was possible to describe the data by fitting a single exponential function to the data and obtained average lifetimes of ~30 µs and ~40 µs for their 295 K and 7 K measurements, respectively. These lifetimes are interpreted to reflect the excited state lifetime of the $IRPL_{955}$ defect at the two different temperatures measured. Kumar et al. (2020) performed TCSPC based lifetime measurements on one feldspar sediment extract (R47), which was also investigated by Prasad et al. (2017). Kumar et al. (2020) obtained lifetimes of 20 µs for the off-time for both $IRPL_{880}$ and $IRPL_{955}$ signals at room temperature, which is faster than the lifetime obtained by Prasad et al. (2017) for the same sample. Besides the two studies by Prasad et al. (2017) and Kumar et al. (2020) no detailed investigations have been made into the lifetimes of the $IRPL_{880}$ and $IRPL_{955}$ emissions.

Here we aim at investigating the dependence of IRPL lifetime, which is a fundamental characteristic of the electron trapping centre, describing its excited state to ground state transition, on composition and structure of selected alkali feldspars. To further constrain our understanding of the processes influencing the lifetime, we also investigate the effect of preheating at different temperatures on the $IRPL_{880}$ and $IRPL_{955}$ lifetimes.

2 Material and methods

2.1 Sample material

A suite of eleven chemically and structurally different single crystal alkali feldspar samples, including K- and Na-feldspar end members was used in this study. The samples investigated here reflect the range of alkali feldspars found in nature. Ordered single phase feldspars, with microcline as the K-feldspar end member and albite as the Na-feldspar end member, are rather rare occurrences. In these

crystals Si^{4+} and Al^{3+} tetrahedra form the framework, whilst K^+ and Na^+ ions are located in the cavities of the framework. Whilst end members contain one type of these cations (either Na^+ or K^+), perthites contain both. The difference in ionic radii of K^+ and Na^+ ions drive the formation of exsolution lamellae in perthitic feldspars during cooling of rocks. Whilst all of these described feldspars form during slower cooling, for instance in igneous or metamorphic rocks, disordered feldspars form by rapid cooling in e.g. volcanic rocks, during which the high temperature structural state (disorder of Si^{4+} and Al^{3+} ions on the framework) of the feldspar is retained (Deer et al., 2013).

Details regarding the samples' origin, their chemical composition, and on the mineral phases present in the specimens are given in Table 1. The chemical composition (relative contribution of the main feldspar phases, %) was determined from quantitative X-ray fluorescence (XRF) data using stoichiometry. Semi-quantitative phase analysis results are based on X-ray diffraction (XRD) data. Details on the instrumentation used for XRF and XRD measurements are explained in Riedesel et al. (2021b). Samples FSM-13LH and FSM-6LH are artificially disordered counterparts of samples FSM-13 and FSM-6. FSM-13LH and FSM-6LH were heated to 1050 °C in a furnace for 5 days (FSM-6LH) and 10 days (FSM-13LH) to disorder the (Si,Al)-framework. To retain the disordered structure the samples were rapidly cooled to room temperature. The disordered structure was validated using XRD. Further details regarding this experiment and the obtained X-ray diffraction patterns can be found in Riedesel (2020) and Riedesel et al. (2021b). The luminescence behaviour of the samples has been studied previously and results from excitation and emission spectroscopy of the samples can be found in Riedesel et al. (2019, 2021a and 2021b). Time-resolved IRSL measurements were also performed on some of the samples and the results are presented in Riedesel et al. (2023).

2.1 Instrumentation

All time-resolved measurements were made on a Risø TL/OSL DA20 reader located at the Radiation Physics Division, Department of Physics, Technical University of Denmark. The luminescence reader is equipped with a $^{90}Sr/^{90}Y$ source delivering ~0,1 Gy s^{-1} at sample position. The luminescence is excited by using an IR (830 nm) 140 mW TTL modulated laser passing through a diffuser to obtain a uniform power distribution on the sample disc. The emitted luminescence is detected by a Hamamatsu H7421-50 (380-890 nm) PMT through a combination of two LP850 and LP880/10 nm BP filters for the $IRPL_{880}$ emission and by a Hamamatsu H10330C-25 (950-1200 nm) PMT through a combination of two LP925 and 950/50AP BP filters to isolate the $IRPL_{955}$ emission.

Table 1. Details regarding the chemical composition and mineral phases present for samples investigated. The chemical composition in % feldspars, was calculated from semi-quantitative XRF data using stoichiometric conversion. Mineral phases present were estimated based on semi-quantitative XRD analyses.

Sample ID	Origin	Chemical composition (FS %)			Phases present			
		K-FS	Na-FS	Ca-FS	Microcline	Orthoclase	Sanidine	Albite
FSM-13	Brazil	98.5	1.5	0.0	100.0	-	-	
FSM-13LH	Brazil	98.5	1.5	0.0	100.0	-	-	
FSM-3	Granite pegmatite, Toe Head, South Harris, Scotland, UK (Cunningham, 1981)	82.5	17.2	0.3	78.0	-	-	22.0
FSM-15	Buckingham, Quebec, Canada	80.4	19.6	0.0	82.0	-	-	18.0
FSM-7	Unknown	76.8	22.0	1.2	48.0	-	-	51.0
FSM-5	Unknown	74.8	25.20	0.0	57.0	-	-	43.0
FSM-6	Granite pegmatite, Trezaise Quarry, Cornwall, UK (Ussher et al., 1909)	74.4	25.3	0.3	-	38.0	-	62.0
FSM-6LH	Trezaise Quarry, Cornwall, UK	74.4	25.3	0.3	-	-	100.0	-
FSM-11	Perth, Canada	65.2	34.8	0.0	62.0	-	-	38.0
Al-I	Pinzele, Trente, Italy (Govindaraju, 1995)	1.0	97.0	2.0	-	-	-	-
CLBR	Pegmatite, Golonca District, Minas Gerais, Brazil (Cassadanne and Roditi, 1996)	0.5	99.3	0.2	-	-	-	100

2.2 Experimental setup

Two different measurement protocols were used to gain insights into the lifetimes and the stability of the $IRPL_{880}$ and $IRPL_{955}$ signals and the two protocols are outlined in Tables 2 and Table 3. The same aliquots were used for all measurements and two aliquots were measured per sample. The aliquots were made by placing the sample (either as shards or powder) on the stainless-steel cups. No adhesive agent was used.

To minimise the potential influence of sensitivity change on the measurement results, all aliquots were stimulated with two consecutive IRSL measurements at 290°C ($IRSL_{290}$) for 100s prior to the first pulsed IRPL measurement. The second of these consecutive $IRSL_{290}$ measurements served as a measure for any potential remaining background signal, which was found to be negligible for all samples. Following the $IRSL_{290}$ bleach the samples were given a 5 Gy beta dose before performing the remaining TL, IRSL and/or IRPL measurements.

The first measurement protocol (Table 2) was used to measure the lifetimes of the $IRPL_{880}$ and $IRPL_{955}$ signals following a preheat at 250 °C for 60 s using three different on-time durations (pulse width) for the 830 nm laser stimulation (5, 10 and 20 µs). The protocol outlined in Tables 3 test for the lifetime dependence of the $IRPL_{880}$ and $IRPL_{955}$ signals on prior heating (after dose).

Table 2. Measurement protocol for time-resolved IRPL signals after a preheat at 250 °C, with different on-time durations. On-time duration of 5, 10 and 20 µs were tested for time-resolved IRPL signals.

Step	Treatment
1	CW-IRSL at 290 °C for 100 s (bleach)
2	CW-IRSL at 290 °C for 100 s (bleach)
3	5 Gy beta dose
4	TL at 250 °C for 60 s, 2 °C/s
5	Time-resolved $IRPL_{880}$ for 10 s at 30 °C
6	Time-resolved $IRPL_{955}$ for 10 s at 30 °C

Table 3. Measurement protocol for pulse anneal experiments.

Step	Treatment
1	CW-IRSL at 290 °C for 100 s (bleach)
2	CW- IRSL at 290 °C for 100 s (bleach)
3	$IRPL_{880}$ for 10 s at 30 °C, On-time: 20 µs, Off-time: 80 µs
4	$IRPL_{955}$ for 10 s at 30 °C, On-time: 20 µs, Off-time: 80 µs
5	5 Gy beta dose
6	TL to 50 at 2°C/s
7	$IRPL_{880}$ for 10 s at 30 °C, On-time: 20 µs, Off-time: 80 µs
8	$IRPL_{955}$ for 10 s at 30 °C, On-time: 20 µs, Off-time: 80 µs
	Return to step 6 and increment TL temperature by 50C (until 600C).

2.3 Fitting

Fitting of time-resolved luminescence signals was done in R using a non-linear least square fitting approach, facilitating the nls() function (Bates and DeRoy, 2018) and using equation 1 for the off-time signal. Here I is the intensity at time t, a_i the intensity at time t_1, where t_1 is the on-time duration, and k is a constant, representing a stable linear background (e.g. Demas, 1983, p. 39; Chithambo, 2003; Tsukamoto et al., 2006). The data were normalised to the intensity of the last data point of the on-time.

$$I(t) = \sum a_i \exp\left[-\left(\frac{t-t_1}{\tau_1}\right)\right] + k \qquad [1]$$

To obtain information on the contribution of each lifetime to the total off-time signal, we integrated the area under each exponential function and normalised the obtained integral to the sum of the three integrals for each sample to obtain the relative contribution for each component.

3 Influence of experimental setup on time-resolved IRPL

Prior to investigating sample-dependent variations of the time-resolved IRPL signals and their response to increasing preheat temperatures, we conducted experiments monitoring the effects of the instrument setup and the experimental conditions. We specifically evaluate different ways of removing the laser breakthrough from the actual IRPL signal (section 3.1) and discuss variations in $IRPL_{880}$ and $IRPL_{955}$ lifetimes with on-time duration (section 3.2).

3.1 Removal of stimulation light breakthrough in the $IRPL_{880}$ signal

In our measurement system, the laser switch-off is not instantaneous. Instead, there is an afterglow lasting a few microseconds. Due to the proximity of the excitation light source (830 nm laser) and the detection window for the $IRPL_{880}$ emission (880 nm ± 5 nm at FWHM) an emission from the stimulation light source is also detected. This signal contaminates the recorded $IRPL_{880}$ emission (cf. Fig. 1a, b), and the influence can be significant in samples with low $IRPL_{880}$ intensity. In the case of IRPL measurements performed in geochronological studies, the pulsing of the laser is enabled, and the off-time signal used for age calculation is recorded as gated signal after discarding the initial 1 µs (Kumar et al., 2021) or the initial 3 µs (Kook et al., 2017) of the off-time. However, in case of the present study, we are interested in the full off-time signal to make an accurate estimate for any fast-decaying IRPL components. Therefore, it becomes pertinent to characterise the decrease in the intensity of the stimulation laser light pulse in the off-time. This breakthrough also places a limit on the minimum detectable IRPL lifetime in our system.

Table 4. $IRPL_{880}$ lifetimes obtained for the laser on different substrates. I represents the intensity of each component, τ the lifetime and A the amplitude (integrated area under the fitted curve). The different components are denoted using an index number. Prior to fitting the signals were normalised to the last data point of the on-time.

Substrate	I_1	τ_1	A_1	I_2	τ_2	A_2	I_3	τ_3	A_3
Empty cup	1.04	0.10	0.10	0.09	1.59	0.14	0.01	10.0	0.10
Shard	1.03	0.10	0.10	0.08	1.69	0.14	0.02	14.6	0.29
Powder	1.06	0.10	0.11	0.08	1.7	0.14	0.01	15.02	0.15

To constrain the lifetime of the laser off-time we measured the response of the laser on an empty cup and on cups filled with non-$IRPL_{880}$ emitting sample material in the form of powder (Al-I) or shards (CLBR, see Riedesel et al., 2021a for emission spectra, which reveal that this feldspar does not exhibit an $IRPL_{880}$ emission). The signal was recorded according to the procedure outlined in Table 2, using an

on-time duration of 20 µs and an off-time duration of 80 µs. Figure 1c shows the 830 nm laser breakthrough emission recorded on different substrates, with slightly higher on-time intensities recorded for the powdered material, likely due to surface-dependent scattering of the incoming laser light. When fitted using equation 1 three lifetime components can be obtained for all three cups and materials tested. The fastest lifetime component (hereafter referred to as lifetime 1, τ_1) dominates the signal with 91 % of the initial signal intensity. τ_1 decays with a lifetime of 0.1 µs. The two slower lifetime components make up the remaining 9% of initial signal with τ_2 decaying with a time 1.6 µs and τ_3 at 12.7 µs (cf. Fig. 1d, Table 4).

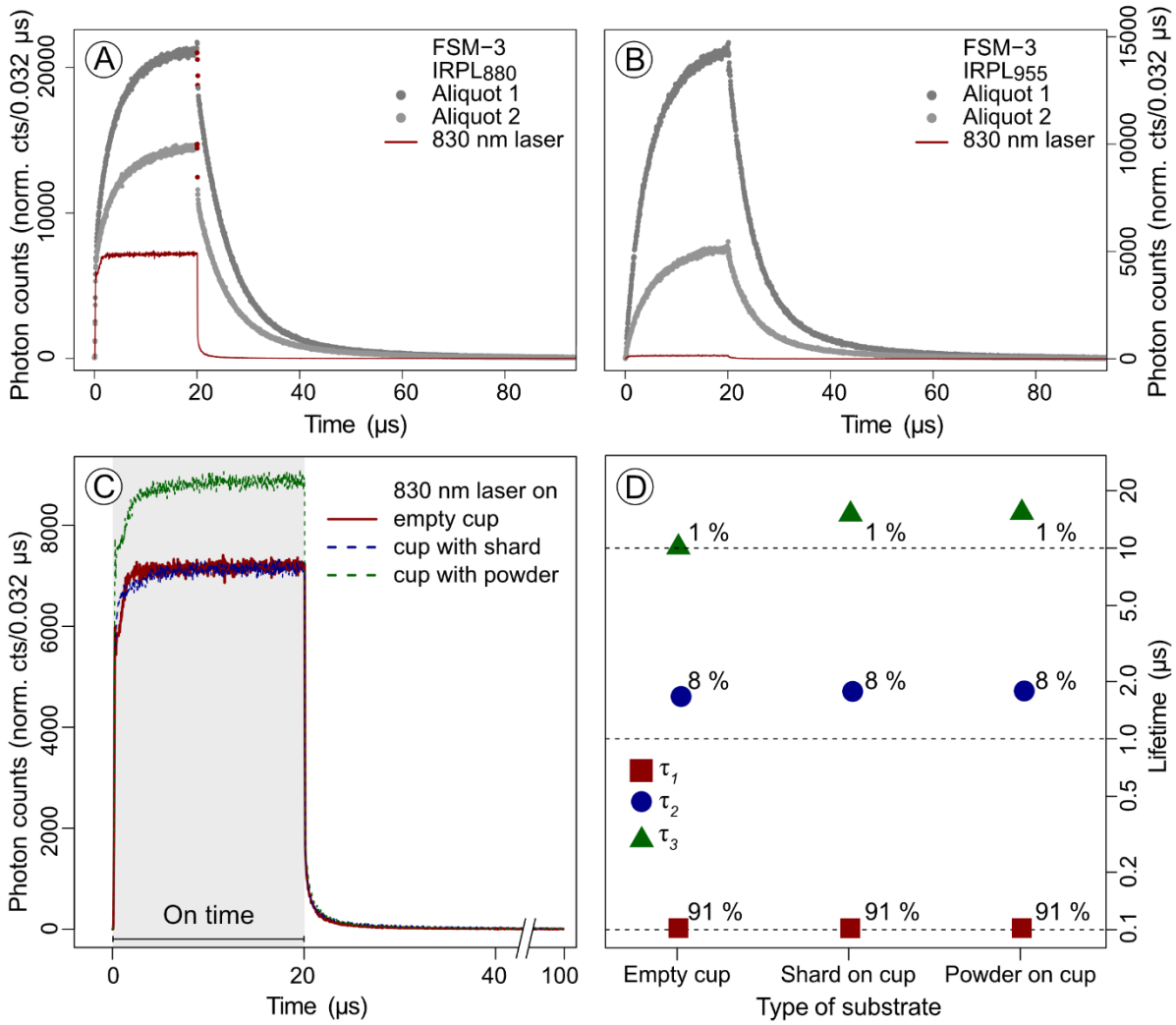

Fig. 1. Comparison of IRPL$_{880}$ (A) and IRPL$_{955}$ (B) emissions of sample FSM-3 with that of the laser breakthrough recorded for an empty cup. The red dots in the IRPL$_{880}$ emission of sample FSM-3 represent the part of the sample signal influenced by the laser breakthrough C) Recorded breakthrough of 830 nm stimulation laser on different substrates for IRPL$_{880}$. The IR laser breakthrough was measured on an empty cup (red line) and on different types of non-IRPL emitting sample material on cups. The latter include a single shard (sample CLBR)

and powder (samples Al-I). C) Apparent lifetimes of the laser breakthrough signal in the off-time obtained by fitting a sum of three exponential functions for the different substrates.

When comparing the time-resolved $IRPL_{880}$ signal from a sample, in this case FSM-3 (cf. Fig. 1a), to the laser breakthrough, one can see that especially the fastest laser lifetime (τ_1) influences the initial off-time decay of the feldspar sample. To highlight this, the data points reflecting the laser breakthrough are highlighted in red in Fig. 1A. Thus, it is important to deal with this contaminating laser signal to be able to estimate the off-time IRPL decay lifetime(s). We tested three different approaches and compared the results for $IRPL_{880}$ signal from five different feldspar samples: FSM-3, FSM-7, FSM-11, FSM-13LH and FSM-15 (Fig. 2). These samples were chosen because of their varying $IRPL_{880}$ intensities, thus, enabling us to test the effect of different breakthrough removal approaches on differently luminescent samples.

Firstly, we fitted the $IRPL_{880}$ off-time signal of those five samples using equation 1 and a sum of three exponential functions. The results are used as reference for all three laser removal approaches as described below:

1. As a first approach to remove the laser breakthrough we subtracted the actual laser signal (not the fitted signals) recorded on an empty cup from the sample specific $IRPL_{880}$ signal and fitted the thus obtained signal using the sum of three exponential functions. As shown in Figure 1c, the laser signal intensity depends on the light scattering from the sample. Subtracting the laser signal from the sample signal results in negative on-time signal intensities for all samples, which is reflected in a negative intensity (I) of τ_1 in the case of all samples. The intensity is not displayed in Fig. 2, but the column where this is the case is highlighted in Fig. 2.

2. As a second removal approach, we systematically excluded initial data from the off-time signal prior to fitting. The time-resolved data is integrated over bins with a width of 0.032 µs. Selecting channels to be excluded from the signal are thus dependent on this binning structure. We considered data removal corresponding to five different time intervals ranging from 0.256 µs up to 3 µs. We removed the first eight, sixteen and 25 channels of the off time (0.256 µs, 0.512 µs and 0.738 µs). In line with the suggestions by Kumar et al. (2020) and Kook et al. (2017) we also tested removing the initial 1 µs and 3 µs, respectively. When using this approach, the number and decay time of the fitted lifetimes vary for each sample (Fig. 2). Removing initial channels from the fitted off-time data affects mostly the presence and lifetime of τ_1. τ_1 is completely removed in samples FSM-3 and FSM-13LH. In samples FSM-7, FSM-11 and FSM-15 τ_1 becomes slower until it is fully removed with sufficient exclusion of the initial off-time signal. The other two lifetimes are nearly unaffected in case of FSM-3, FSM-11, FSM-7 and

FSM-15. For τ_2 and τ_3 these samples experience a change in lifetime of 1 to 2 dependent on the sample and lifetime. In case of FSM-13LH the removal of the initial 1 µs results in τ_2 doubling compared to the measurement without signal removal. Removing the initial 3 µs results in an increase of τ_2 from prior 1-2 µs to over 8 µs. Looking at these results, the approach of removing initial parts of the off-time signal, might be questionable, when investigating the time-resolved IRPL signals. However, for dating purposes removing the initial 1 µs, as suggested by Kumar et al. (2020) will be a useful practicality, as this removes most of the laser breakthrough light, whilst still having sufficient off-time IRPL signal remaining for performing the dating procedure.

3. As a last test, we fixed τ_1 in all samples to 0.1 µs (the value obtained for the laser breakthrough on an empty cup and material without $IRPL_{880}$ emission) while leaving the other two lifetimes free during the fitting procedure. When comparing the obtained lifetimes of τ_2 and τ_3 for the five samples we observe similar results to those obtained when all parameters are left free during the least square fitting approach (cf. Fig. 2).

We thus decided to use the approach of fixing τ_1 to 0.1 µs for all further data analysis in the study because (i) it helps us in objectively removing the largest impact of the laser breakthrough, (ii) despite fixing the first lifetime we still obtain lifetimes for τ_2 and τ_3 close to the value obtained when fitting the entire off-time and leaving all fitting parameters free during the fitting procedure and (iii) it treats all samples equally, thus hopefully allowing an objective analysis of our results.

Since the breakthrough of the 830 nm laser is minimal for the $IRPL_{955}$ detection value, we decided to leave all lifetimes free to vary in the fitting approach of the $IRPL_{955}$ signal.

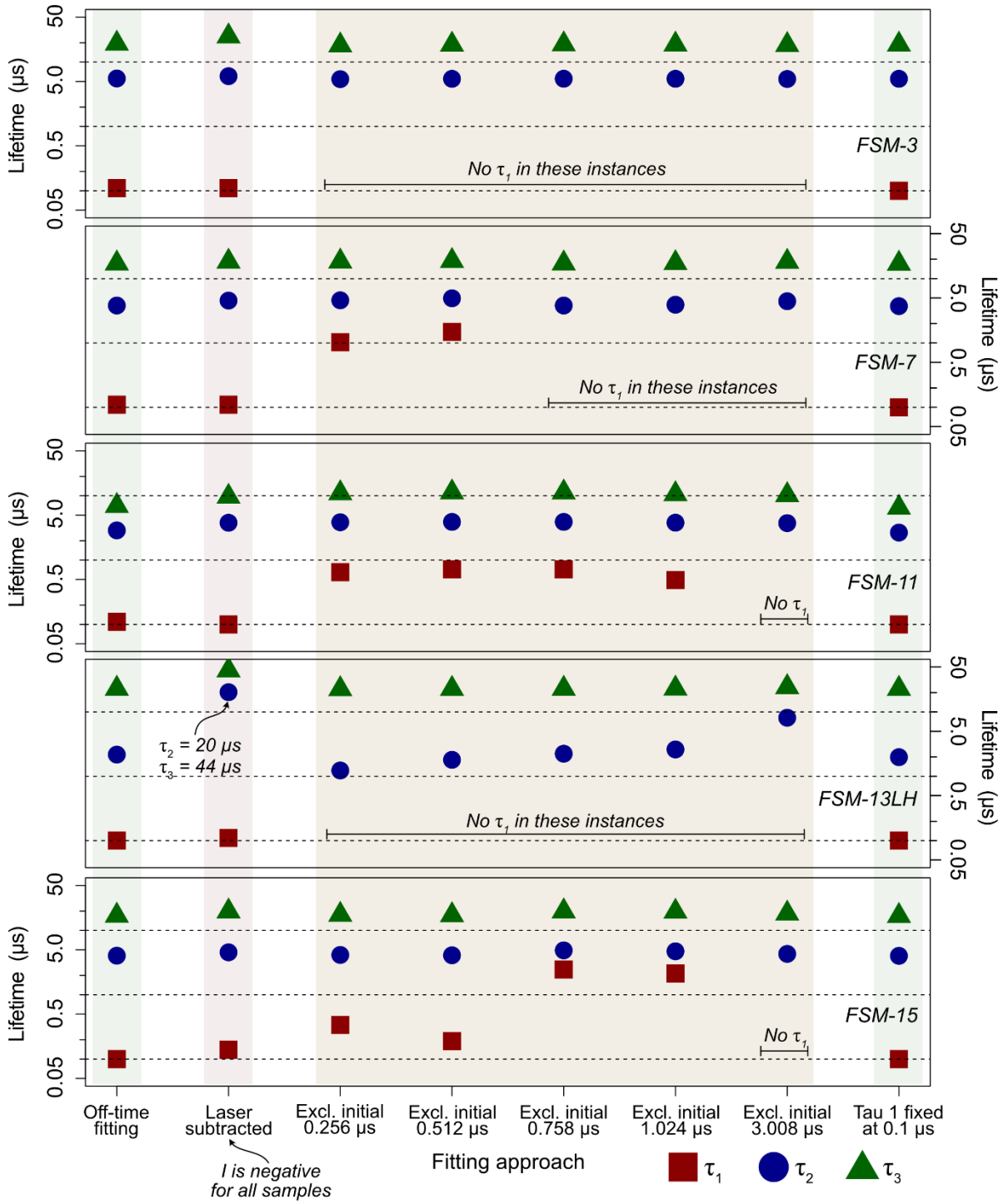

Fig. 2. To remove the influence of the laser signal on the IRPL880 emission of the sample, different extraction methods were tested on aliquots from five different samples. "Off-time fitting" refers to fitting of the signal off-time, without any further modifications. For the "Laser subtracted" column the laser signal measured on an empty cup was subtracted from the signal recorded for the sample. For the steps referring to the exclusion of the initial signals, successive channels were removed from the initial off-time signal, aiming at isolating the signal, which is independent of the laser. As the last step, the first lifetime (tau 1) was fixed to 0.1 µs for fitting, whilst the other two lifetimes were left to vary freely. Each point represents one aliquots of each sample.

3.2 On-time durations

During the on-time the signal rises gradually according to its characteristic lifetime; in the limiting case the signal reaches a steady state (plateau). This implies that the ratio of IRPL signal to the breakthrough will be a function of the on-time duration. Thus, in order to confirm the accuracy of our analysis, we test the influence of the on-time duration on the lifetime measurements. For this experiment we used the protocol described in Table 2 on all eleven feldspar samples to test on-time durations of 5 µs and 10 µs against 20 µs, as used in section 3.1. The breakthrough contamination relative to the signal will decrease systematically from 5 µs to 20 µs. The off-time decay was fitted using equation 1 and the sum of three exponential function, while fixing τ_1 to 0.1 µs for the $IRPL_{880}$ signal.

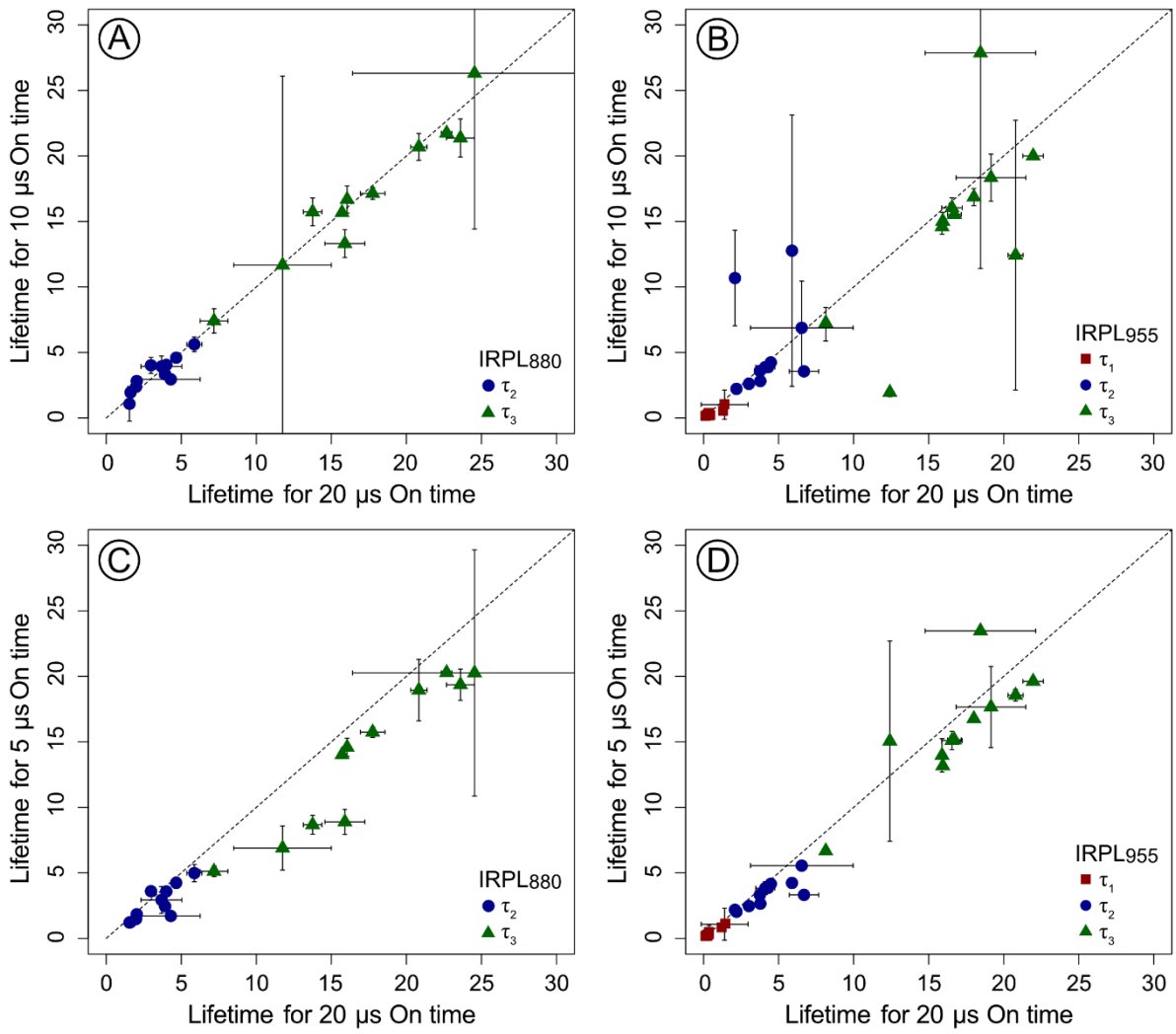

Fig. 3. Comparison of off-time lifetimes recorded after different durations of off-times. A) 20 µs compared to 10 µs for $IRPL_{880}$. B) 20 µs compared to 10 µs for $IRPL_{955}$. C) 20 µs compared to 5 µs for $IRPL_{880}$. D) 20 µs compared to 5 µs $IRPL_{955}$. Each data point is the average of two aliquots per sample and the standard deviation.

Figure 3 shows the comparison of the fitted $IRPL_{880}$ (Fig. 3a,c) and $IRPL_{955}$ (Fig. 3b,d) lifetimes measured suing different on-time durations. The dotted line represents the 1:1 line. The lifetimes derived from the 10 µs on-time data are indistinguishable from those for 20 µs data (Figure 3a,b). However, the 5 µs data tends to under-estimate the latter (Figure 3c,d). This tendency is much stronger for $IRPL_{880}$ signal where we have much larger breakthrough. The larger scatter observed for the $IRPL_{955}$ data is presumably due to its lower intensity. Since a visible change in lifetimes can be obtained when decreasing the on-time from 20 µs/10 µs down to 5 µs in the further course of this study an on-time of 20 µs is used. An off-time of 80 µs is sufficient in the case of all samples to reach a stable background level prior to the next stimulation pulse.

Based on the observations outlined in section 3.1 and 3.2, all measurements were done with an on-time of 20 µs and an off-time of 80 µs, and the fitting analysis included three exponential components, with the first component assigned a fixed lifetime of 0.1 µs in case of $IRPL_{880}$. In case of the $IRPL_{955}$ all lifetimes were kept free during fitting.

4 Factors influencing the lifetimes of the IRPL signals

In the following we compare the $IRPL_{880}$ and $IRPL_{955}$ signal intensities and lifetimes (section 4.1). We then proceed to present and discuss the dependence of $IRPL_{880}$ and $IRPL_{955}$ lifetimes on the sample composition (section 4.2) and which effect pulse annealing (i.e. preheating) has on the excited state lifetimes (section 4.3).

4.1 Comparison of $IRPL_{880}$ and $IRPL_{955}$ signals

Figure 4A shows a linear relationship between the off-time signal intensity of both the IRPL signals, as has also been reported in previous work (Jain et al., 2020). The intensity of the laser breakthrough is indicated in Fig. 4A.

When comparing lifetimes between $IRPL_{880}$ and $IRPL_{955}$ signals for different samples, we observe that τ_2 is uncorrelated, whereas τ_3 perhaps shows a weak trend between the two IRPL signals (cf. Fig. 4B,C). However, both albite specimen CLBR and Al-I and perthitic feldspar FSM-11 show very weak $IRPL_{880}$ signals The CLBR data confirms previous report by Riedesel et al. (2021a). Since Al-I is also a single-phase feldspar, similar behaviour to CLBR was expected. We cannot explain why FSM-11 shows only weak $IRPL_{880}$ signals, but it is interesting to note that this sample also shows much faster τ_3, with both aliquots showing off-time lifetimes of <10 µs. If one rejects these three samples based on the ground of poor sensitivity, and hence the possibility of contamination by the laser (highlighted in figure 4C), then there is a cluster of no clear correlation between τ_3 values, broadly consistent with 1:1 line,

suggesting that both the $IRPL_{880}$ and $IRPL_{955}$ centres have a common lifetime of the dominant component of the IRPL signal, i.e. the slowest component (τ_3).

All other samples show τ_2 and τ_3 lifetimes in defined ranges. τ_2 ranges from 1.99 ± 0.06 (FSM-6LH) to 5.87 ± 0.50 (FSM-3) for $IRPL_{880}$ and from 3.75 ± 0.05 (FSM-15) to 6.69 ± 0.98 (FSM-13LH) for $IRPL_{955}$. τ_3 ranges from 15.71 ± 0.05 to 24.54 ± 8.13 for $IRPL_{880}$ and from 15.89 ± 0.08 to 20.79 ± 0.5 for $IRPL_{955}$. Please note that these are the average (± standard deviation) of the two aliquots measured per sample. For illustration purposes we displayed the lifetimes measured for each aliquot in Fig. 4. Another interesting observation is that for weakly luminescent samples we observe a small dependency of the lifetime on the intensity of the signal, which is more pronounced for the $IRPL_{880}$ signal than for the $IRPL_{955}$ signal (see Fig. S5 in the supplementary material). This could potentially indicate that the laser breakthrough impacts the lifetime slightly in case of the dimmer samples. However, since lifetimes measured for $IRPL_{880}$ and $IRPL_{955}$ emissions are similar in each sample (Fig. 4B, C), we still consider our results to be valid. We will, however, disregard the $IRPL_{880}$ results of albite specimen CLBR and Al-I due to the lack of an $IRPL_{880}$ emission. FSM-11, although it shows only very weak $IRPL_{880}$ emission, the off-time decay is very different to the laser breakthrough (see Fig. S4I, J). Thus, we will still include this sample in our discussion.

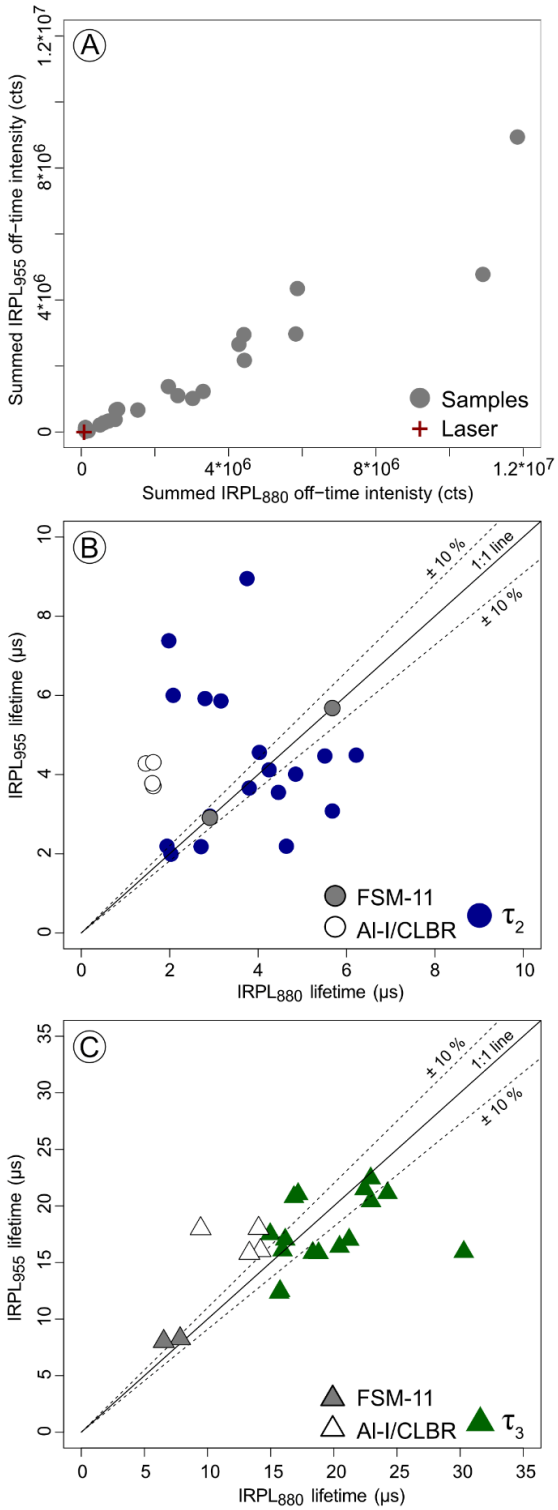

Fig. 4. (A) Comparison of the $IRPL_{880}$ and $IRPL_{955}$ signal intensities. For this plot the entire off-time signal for each emission was integrated. (B) Comparison of τ_2 for the off-time of $IRPL_{880}$ and $IRPL_{955}$. (C) Comparison of τ_3 for the off-time of $IRPL_{880}$ and $IRPL_{955}$. A one-to-one line and 10 % deviation from this line are indicated in B and C.

4.2 Influence of feldspar chemistry and structure on IRPL lifetimes

Here we explore potential effects of the sample chemistry and structural state on the IRPL lifetimes. To visualise the results, the samples and their recorded lifetimes were ranked according to the samples K-feldspar content (Fig. 5). The summed off-time intensity is displayed in Fig. 5A and C. Here the intensity of the individual aliquots measured per sample are shown. The relative integral contribution from each lifetime to the overall off-time signal is visualised in the size of the data points (Fig. 5C, D), where each data point represents the average of two aliquots. The numerical fitting results are given in Tables 5 and 6 for the $IRPL_{880}$ and $IRPL_{955}$ signals, respectively.

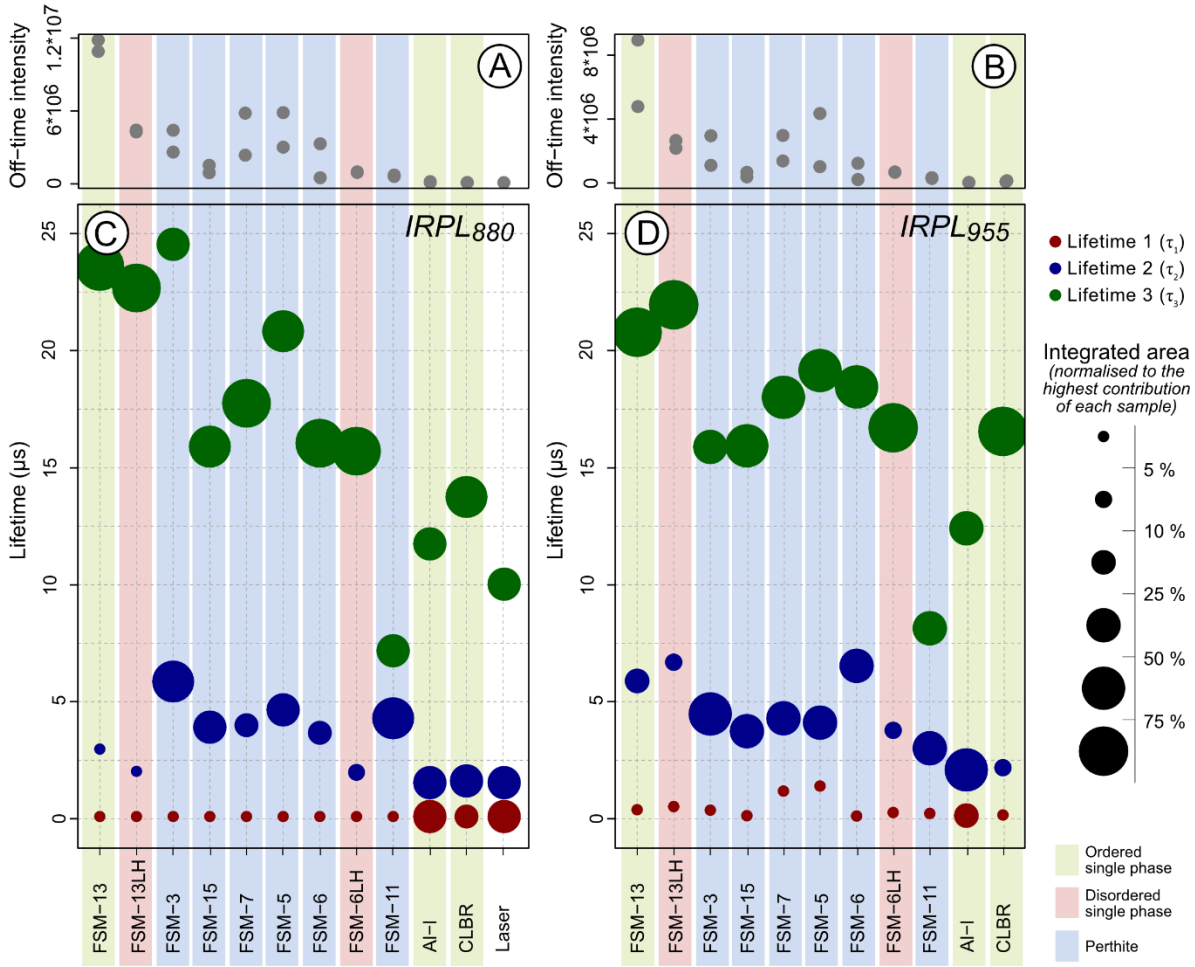

Fig. 5. Intensities of total integrated off-time signals for $IRPL_{880}$ (A) and $IRPL_{955}$ (B). Lifetimes obtained through fitting using the sum of three exponential functions for the $IRPL_{880}$ (C) and $IRPL_{955}$ signals (D). The results are ordered according to each sample's K-feldspar content (KFS, %). Each data point is the average of two aliquots per sample. Uncertainties are not displayed but can be taken from table 6 and 7 for $IRPL_{880}$ and $IRPL_{955}$, respectively. The size of the points corresponds to the integrated area under the exponential function for each lifetime. The integrated area for each lifetime was normalised to total area, i.e. the sum of three exponentials, for each sample.

IRPL$_{880}$ lifetimes

Although τ_1 can be ignored in case of the IRPL$_{880}$ signal, it is worth mentioning that when comparing the relative contributions of each lifetime to the total integrated off-time signal, τ_1 contributes to less than 5 % to the total signal in case of most samples. The only exceptions are single-phase albite specimens Al-I and CLBR. Here τ_1 contributes to 30 % and 20 % to the overall IRPL$_{880}$ off-time signal, respectively. However, when looking at the photon arrival time distributions of these two samples (Fig. S3) and by keeping in mind that Riedesel et al. (2021b) showed that single-phase Albite CLBR did not exhibit an IRPL$_{880}$ signal, the IRPL$_{880}$ results, at least of CLBR, likely also of Al-I, have only little relevance for the data interpretation. Consequently, the IRPL$_{880}$ signal of samples CLBR and Al-I is not further considered. For transparency reasons they are still displayed in Fig. 5.

In the remaining nine alkali feldspar samples investigated, including FSM-11, τ_2 shows lifetimes ranging from 1.99 ± 0.06 (FSM-6LH) to 5.87 ± 0.50 (FSM-3). The relative contribution of τ_2 to the overall off-time signal also depends on the sample, with τ_2 making up less than 2 % of the total signal in samples FSM-13 and FSM-13LH, and only 7 % in the third single-phase feldspar FSM-6LH. Interestingly, all three samples are single-phase feldspars. In perthitic samples FSM-3 and FSM-11, τ_2 is the dominating lifetime component, with contributing to 67 % and 50 %, respectively.

τ_3 is the dominant lifetime component in most samples, with the exception of FSM-3 and FSM-11. In all other samples τ_3 contributes to at least 50 % to the overall signal. In samples FSM-13 and FSM-13LH τ_3 makes up nearly 100 % of the total off-time signal. When comparing τ_3 for all samples in relation to their K-feldspar content, then one can observe a general trend of decreasing τ_3 lifetime with decreasing K-feldspar content of the sample (Fig. 5C). Please note that there is no linear axis scale for the K-feldspar content in Fig. 5C. The samples are just ordered according to their K-feldspar content. For the actual K-feldspar content please refer to Table 1.

IRPL$_{955}$ lifetimes

For the IRPL$_{955}$ signal all three lifetimes can be investigated (Table 6, Fig. 5B). Here, τ_1 ranges from 0.14 ± 0.01 µs (single phase albite Al-I) to 1.4 ± 1.56 µs (macroperthite FSM-5), with FSM-5 and FSM-7 being the only samples exhibiting τ_1 times slower than 1 µs. Similarly to IRPL$_{880}$, τ_1 has the smallest contribution to the overall IRPL$_{955}$ off-time signal, making up less than 5 % of the total signal in all samples, except for single-phase albite Al-I. Here τ_1 contributes to ~1/5th of the overall signal.

In case of the IRPL$_{955}$ signal τ_2 ranges from 2.09 ± 0.14 µs (single phase albite Al-I) to 6.69 ± 0.98 µs (disordered K-feldspar FSM-13LH). The contribution of τ_2 to the IRPL$_{955}$ off-time signal ranges from ~8 to ~9 % (disordered samples FSM-13LH and FSM-6LH, single-phase albite CLBR) to over 50 % (Al-I). τ_2

is the dominant lifetime in case of perthites FSM-3 (53 %) and FSM-11 (49 %) and single-phase albite Al-I (53 %).

τ_3 ranges from 8.14 ± 0.17 µs (perthite FSM-11) to 21.96 ± 0.68 µs (disordered signal-phase sample FSM-13LH). Only FSM-11 and single-phase albite Al-I (12.41 ± 0.11 µs) exhibit τ_3 lifetimes faster than 15 µs. The longest lifetime is dominant in most samples but contributes to at least 28 % of the total signal in case of all samples.

A sample-to-sample comparison of the three different lifetimes obtained from fitting the $IRPL_{955}$ off-time signal, shows weak dependence of τ_3 on the sample's K-feldspar content. When comparing the ordered and disordered sample pairs no trend, as visible for $IRPL_{880}$, can be observed for the $IRPL_{955}$ signal. Whilst τ_2 and τ_3 increase from FSM-13 to FSM-13 LH, a decrease in lifetime for τ_3 and τ_3 can be observed when disordering FSM-6 to FSM-6LH.

*Table 5. $IRPL_{880}$ lifetimes obtained for all samples investigated by fitting the off-time decay of the $IRPL_{880}$ with the sum of three exponential functions, with the first lifetime being fixed to 0.1 µs. The values in the table are the average and standard deviation of two aliquots, which were measured per sample. I represents the intensity of each component, τ the lifetime and A the amplitude (integrated area under the fitted curve). The different components are denoted using an index number. Prior to fitting the signals were normalised to the last data point of the on-time. *The small contribution of τ_2 and τ_3 for samples CLBR and Al-I shows that these samples basically show no $IRPL_{880}$ emission and that the signal consists of the laser breakthrough only (see also Fig. 1 for details). We thus exclude the $IRPL_{880}$ results of Al-I and CLBR from our discussions.*

Sample ID	KFS [%]	I_1	τ_1 [µs]	A_1 [%]	I_2	τ_2 [µs]	A_2 [%]	I_3	τ_3 [µs]	A_3 [%]
FSM-13	98.5	0.21 ± 0.01	0.10 ± 0.00	0.12 ± 0.02	0.09 ± 0.10	2.98 ± 0.25	1.64 ± 0.37	0.73 ± 0.02	23.60 ± 0.93	98.24 ± 0.38
FSM-13LH	98.5	0.56 ± 0.02	0.10 ± 0.00	0.52 ± 0.04	0.06 ± 0.06	2.03 ± 0.07	1.15 ± 0.09	0.46 ± 0.01	22.68 ± 0.35	98.33 ± 0.13
FSM-3	82.5	0.24 ± 0.10	0.10 ± 0.00	0.40 ± 0.21	0.62 ± 0.71	5.87 ± 0.50	66.49 ± 9.3	0.09 ± 0.04	24.54 ± 8.13	33.11 ± 9.09
FSM-15	80.4	0.60 ± 0.08	0.10 ± 0.00	1.91 ± 0.65	0.35 ± 0.38	3.92 ± 0.16	46.42 ± 2.96	0.11 ± 0.02	15.90 ± 1.33	51.67 ± 3.61
FSM-7	76.8	0.35 ± 0.16	0.10 ± 0.00	0.49 ± 0.35	0.38 ± 0.35	4.00 ± 0.35	18.04 ± 1.05	0.36 ± 0.09	17.75 ± 0.82	81.46 ± 1.40
FSM-5	74.8	0.23 ± 0.11	0.10 ± 0.00	0.33 ± 0.21	0.56 ± 0.59	4.66 ± 0.28	37.99 ± 3.17	0.22 ± 0.05	20.83 ± 0.54	61.68 ± 3.38
FSM-6	74.4	0.75 ± 0.35	0.10 ± 0.00	4.03 ± 4.46	0.31 ± 0.19	3.68 ± 1.36	18.55 ± 9.54	0.17 ± 0.13	16.05 ± 0.15	77.42 ± 5.08
FSM-6LH	74.4	0.86 ± 0.00	0.10 ± 0.00	3.00 ± 0.10	0.09 ± 0.10	1.99 ± 0.06	6.58 ± 0.50	0.17 ± 0.01	15.71 ± 0.05	90.42 ± 0.60
FSM-11	65.2	0.66 ± 0.04	0.10 ± 0.00	2.90 ± 0.88	0.27 ± 0.28	4.30 ± 1.96	49.53 ± 8.20	0.16 ± 0.04	7.18 ± 0.92	47.57 ± 7.31
Al-I*	1.0	1.05 ± 0.01	0.10 ± 0.00	29.16 ± 1.45	0.08 ± 0.09	1.55 ± 0.12	38.49 ± 5.50	0.01 ± 0.00	11.75 ± 3.25	32.35 ± 6.95
CLBR*	0.5	1.03 ± 0.00	0.10 ± 0.00	19.97 ± 0.08	0.09 ± 0.09	1.62 ± 0.01	26.70 ± 2.10	0.02 ± 0.00	13.75 ± 0.62	53.33 ± 2.19

Table 6. $IRPL_{955}$ lifetimes obtained for all samples investigated by fitting the off-time decay of the $IRPL_{955}$ with the sum of three exponential functions. The values in the table are the average and standard deviation of two aliquots, which were measured per sample. I represents the intensity of each component, τ the lifetime and A the amplitude (integrated area under the curve). The different components are denoted using an index number. Prior to fitting the signals were normalised to the last data point of the on-time.

Sample ID	KFS [%]	I_1	τ_1 [µs]	A_1 [%]	I_2	τ_2 [µs]	A_2 [%]	I_3	τ_3 [µs]	A_3 [%]
FSM-13	98.5	0.09 ± 0.01	0.39 ± 0.01	0.24 ± 0.05	0.23 ± 0.25	5.89 ± 0.04	10.08 ± 1.87	0.64 ± 0.05	20.79 ± 0.50	89.68 ± 1.92
FSM-13LH	98.5	0.13 ± 0.00	0.53 ± 0.09	0.44 ± 0.07	0.17 ± 0.19	6.69 ± 0.98	8.11 ± 2.02	0.64 ± 0.03	21.96 ± 0.68	91.44 ± 2.09
FSM-3	82.5	0.05 ± 0.04	0.37 ± 0.04	0.28 ± 0.22	0.68 ± 0.74	4.48 ± 0.01	52.69 ± 5.55	0.19 ± 0.02	15.89 ± 0.08	47.02 ± 5.33
FSM-15	80.4	0.43 ± 0.01	0.14 ± 0.01	1.49 ± 0.03	0.51 ± 0.49	3.75 ± 0.05	47.24 ± 3.39	0.13 ± 0.01	15.94 ± 0.18	51.27 ± 3.42
FSM-7	76.8	0.09 ± 0.00	1.19 ± 0.01	1.24 ± 0.04	0.55 ± 0.53	4.30 ± 0.02	26.52 ± 2.29	0.35 ± 0.02	18.01 ± 0.02	72.24 ± 2.33
FSM-5	74.8	0.16 ± 0.06	1.4 ± 1.56	4.08 ± 4.93	0.69 ± 0.65	4.11 ± 0.64	43.86 ± 2.5	0.17 ± 0.01	19.15 ± 2.32	52.06 ± 2.43
FSM-6	74.4	0.87 ± 0.33	0.12 ± 0.00	7.54 ± 7.99	0.30 ± 0.18	6.54 ± 3.42	37.79 ± 9.81	0.10 ± 0.11	18.45 ± 3.68	54.67 ± 17.81
FSM-6LH	74.4	0.24 ± 0.06	0.27 ± 0.08	0.67 ± 0.03	0.23 ± 0.24	3.78 ± 0.33	9.73 ± 1.04	0.50 ± 0.00	16.71 ± 0.45	89.6 ± 1.06
FSM-11	65.2	0.25 ± 0.01	0.23 ± 0.07	1.72 ± 0.48	0.57 ± 0.55	3.02 ± 0.09	49.45 ± 6.08	0.20 ± 0.03	8.14 ± 0.17	48.84 ± 6.56
Al-I	1.0	0.89 ± 0.04	0.14 ± 0.01	18.9 ± 0.5	0.14 ± 0.17	2.09 ± 0.14	52.66 ± 13.36	0.02 ± 0.01	12.41 ± 0.11	28.44 ± 13.86
CLBR	0.5	0.49 ± 0.01	0.17 ± 0.02	1.62 ± 0.47	0.20 ± 0.19	2.19 ± 0.01	8.24 ± 1.76	0.28 ± 0.06	16.55 ± 0.68	90.14 ± 2.23

4.3 Pulse annealing

To test the thermal stability of the IRPL signals and to investigate potential dependencies of the lifetime on the depletion of the trapped charge population, we performed pulse annealing experiments (Table 3) on selected samples: the ordered/disordered sample pairs FSM-13 (single-phase microcline) and FSM-13LH (sanidine) and FSM-6 (perthite) and FSM-6LH (sanidine), as well as two perthites (FSM-3 and FSM-5).

The overall off-time light intensity sum of the pulsed IRPL signals shows a similar trend for both emissions (Figs. 6A and 6B): After irradiating the samples and annealing them to 50 °C all samples, except for macroperthite FSM-5, show a visible increase in $IRPL_{880}$ and $IRPL_{955}$. Riedesel et al. (2021a) already showed that FSM-5, despite showing IRPL emissions centred around 880, 955 and 1020 nm, does not exhibit dose dependent IRPL emissions. The highest signal intensities are observed for sample FSM-6 (perthite) and FSM-6LH (artificially disordered, sanidine). A stable signal plateau is reached during the first measurement cycle (50 °C annealing temperature) and persists until a post irradiation annealing temperature of 400 °C. Following annealing temperatures >400 °C the $IRPL_{880}$ and $IRPL_{955}$ signal intensity decreases for most samples, except for the two artificially disordered samples (FSM-13LH and FSM-6LH). In case of FSM-13LH $IRPL_{880}$ and $IRPL_{955}$ signals remain stable. In case of FSM-6LH a small increase in IRPL intensity is recorded for annealing temperatures at 400 and 450 °C, after which the signal decreases. However, the signal does not reach the initial intensity recorded prior to irradiation (cf. Fig. 6A, B). Interestingly, only pre-annealed (artificially disordered) feldspars show IRPL signals stable >400 °C, indicating that the thermal history of the samples (e.g. their cooling rate in in nature) might influence the thermal stability of the trapped charge population.

To analyse potential changes to the off-time lifetimes of both IRPL signals, the time-resolved signals for each pulse anneal step were fitted following the findings of section 3.1. The results for τ_2 and τ_3 of the $IRPL_{880}$ signal are shown in Fig. 6D and F and for all three lifetimes of the $IRPL_{955}$ signal in Fig. 6C, E and G. The data was normalised to the corresponding lifetime obtained from fitting the off-time signal after an annealing step at 50 °C. The red envelope curve represents the mean of all aliquots and the standard deviation and is displayed for the visualisation of overall trends in the data.

Investigating changes in off-time lifetimes with annealing temperature is challenging due to the scatter in the data (cf. Fig. 6C-G). For τ_2 and τ_3 of both IRPL signals an increasing spread in the data can be observed for annealing temperatures >400 °C. On average τ_2 decreases with increasing preheat temperature for both IRPL signals. In case of individual samples, this decreasing trend is visible for all samples, except for the preannealed samples FSM-13LH and FSM-6LH, in case of $IRPL_{880}$ (Fig. 6D). In $IRPL_{955}$ all samples show a decrease in τ_2 lifetime with increasing temperature (Fig. 6E). τ_3 remains

rather constant throughout the pulse annealing experiment for $IRPL_{880}$ and $IRPL_{955}$. A steady decrease in τ_3 can only be observed for FSM-6.

We associate the larger spread in the data at higher temperature, with a decrease in signal intensity (cf. Fig. 6A,B). Decreasing τ_2 lifetimes, could indicate the impact of laser breakthrough light due to lower $IRPL_{880}$ signal intensities. However, since we observe faster τ_2 lifetimes for $IRPL_{880}$ and for $IRPL_{955}$, we are confident that the observed decrease reflects physical changes in the faster relaxation within the defect. It is interesting to note that on average the longer lifetime component (τ_3) is largely unaffected by increasing preheat temperatures (cf. Fig. 6F, G).

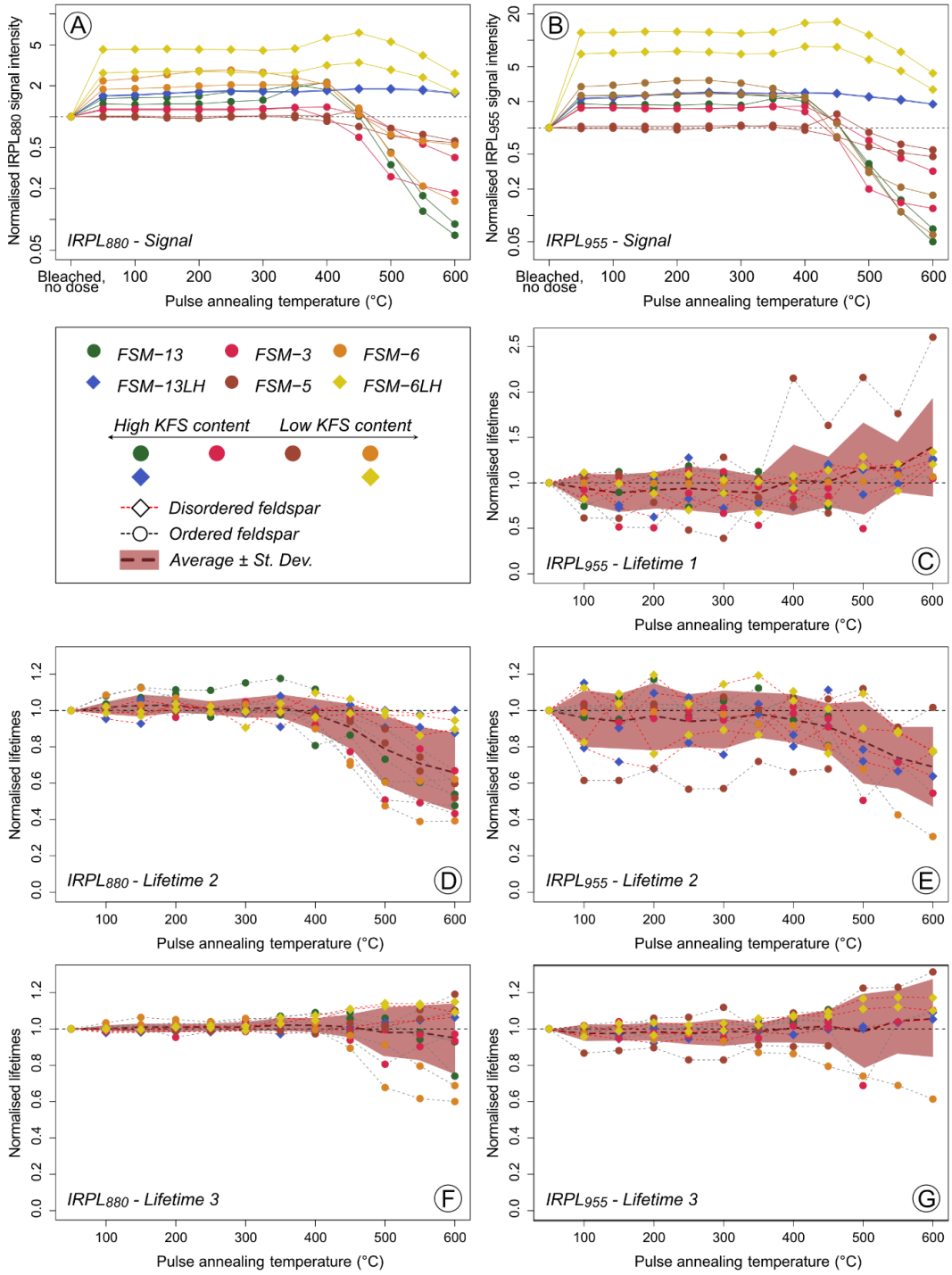

Fig. 6. Pulse annealing test to study the effect of high temperature pre-treatments on the time-resolved $IRPL_{880}$ and $IRPL_{955}$ off-time lifetimes. A), C), E) Pulse annealing experiment results for lifetimes 1 – 3 of $IRPL_{955}$. B) and D) Pulse annealing experiment results for lifetimes 2 and 3 of $IRPL_{880}$. For each sample two aliquots were measured, and the results of measured aliquots are displayed individually. The data is normalised to the lifetime measured after a preheat at 50 °C (first data point of the pulse annealing experiment). For A) and B) the entire off-time signal was integrated to obtain the sum, which was then normalised to the integrated off-

time signal after a CW bleach at 290 °C, prior to administering a beta dose. The red envelope curves represent the mean of all aliquots and the standard deviation.

5 Discussion

5.1 Fitting and single exponential approximation

When fitting our data, we decided on a multi-component fit using the sum of three exponentials as this resulted in the smallest residuals to our fit. We were able to show that the first component (τ_1) represents the dominant part of the stimulation breakthrough light, and we thus excluded it from the $IRPL_{880}$ data. The here observed multi-component decay is interesting, especially because previous research (i.e. Prasad et al., 2017; Kumar et al., 2020) measured only a single lifetime for the IRPL signals studied. When testing different ways of laser breakthrough removal, we found that removing the initial 3 µs of the off-time signal completely removed lifetime τ_1 (Fig. 2). If we use this approach and re-fit the data using a single exponential, we are able to approximate the single component results from Kumar et al. (2020), but only for single-phase feldspars FSM-13, FSM-13LH, FSM-6LH and CLBR (cf. Figs. S6, S7, S9, S10, S11). For all perthites and in case of the weakly luminescent (in the IR) single-phase albite specimen Al-I a clear discrepancy between the fitted exponential curve and the measured data can be seen (Figs. S8, S11), highlighting the sample-dependence of the relative proportions and decay times each lifetime component measured (cf. Fig. 5).

It is expected that a single exponential decay would occur in a simple system with radiative relaxation from the (single) excited state or the lowest excited state to the ground state (e.g. Schlag et al., 1971; Demas, 1983, chapter 3). Multi-component decays can arise from impure samples or from pure samples with complex kinetics (cf. Demas, 1983, chapter 3 and 4). With feldspars we likely study a complex and impure system exhibiting such multi component decays. The two to three component decay could indicate transitions via different closely spaced excited states or the emission from transitions in defects under slightly different crystal environments. To explore this further, spectrally resolved time-resolved measurements would be necessary to monitor changes in lifetime and emission wavelength between samples.

Despite the differences observed in the relative intensities of the various lifetime components, we measured rather tightly clustered lifetimes (Fig. 4B, C), with τ_3 ~20 µs, a result similar to those observed by Kumar et al. (2020).

5.2 Dependencies of measured lifetimes

For our eleven chemically and structurally different alkali feldspars tested we observe a decreasing trend in τ_3 lifetime with decreasing K-feldspar content. This trend is more pronounced in $IRPL_{880}$

compared to $IRPL_{955}$, with single-phase albite specimens CLBR and Al-I not emitting IRPL at 880 nm. In feldspars, cations are located in cavities within the framework. In alkali feldspars this is either K^+ or Na^+, with K^+ having a significantly larger ionic radius than Na^+. The ionic radius of the cation influences bond lengths and framework, with the framework collapsing around the smaller Na^+ ion. This chemically and structurally induced variation in the crystal could potentially explain the trend in measured τ_3 lifetimes with decreasing K-feldspar content. Overall, the lifetimes are rather consistent across the range of alkali feldspars measured, ranging from 16 µs to 25 µs (when dimmest samples are excluded), and thus indicating the same type of defect. A similar consistency was observed in trap depths measurements performed by Kars et al. (2014), Riedesel et al. (2019, 2021a), and Kumar et al. (2020). Due to the similarities in trap depth for the feldspars measured, Riedesel et al. (2019) suggested that the defect acting as electron trapping site in feldspars is located on the framework. A suggestion, which we can support with the here presented data for excited state lifetimes of electron trapping centres in feldspars.

To test whether thermal depletion of the trapped electron population influences the excited state lifetimes we performed a pulse annealing experiment, by measuring IRPL off-time lifetimes following different preheat temperatures. In line with the just described consistencies across the samples investigated, we found that τ_3 is independent of the size of the trapped charge population, which we depleted thermally. Contrastingly, τ_2 decreases with increasing preheat temperature once the preheat temperature exceeds 400 °C. This suggests that the two different excited state lifetimes we measured for the $IRPL_{880}$ and $IRPL_{955}$ signals, respond differently to the thermal depletion of the trapped electron population and that the measurements reflect more than a simple isolated excited state to ground state transition.

5.3 IRPL compared to IRSL lifetimes

IRSL in feldspars is understood as the result from electron-hole recombination (cf. Jain and Ankjærgaard, 2011). Lifetimes obtained for IRSL range mostly from < 1 µs to ~ 20 µs (e.g. Clark et al., 1997; Tsukamoto et al., 2006; Riedesel et al., 2023), with some slower lifetimes being recorded (e.g. Ankjærgaard et al., 2009; Ankjærgaard and Jain, 2020; Riedesel et al., 2023). Faster IRSL than IRPL lifetimes indicate that the leakage from the electron trapping centres to the recombination centres, likely due excited state tunnelling, is faster than relaxation processes within the electron trap itself.

The comparison of published IRSL lifetimes with the here measured IRPL lifetimes suggests three different processes to take place during luminescence production in feldspars: (1) Upon stimulation electrons trapped in electron trapping centres are excited from the ground to the excited state from where they leak to nearby recombination centres via excited state tunnelling (cf. Jain and Ankjærgaard,

2011). This fast leakage is reflected by fast IRSL lifetimes measured elsewhere, but also by τ_2 lifetimes of $IRPL_{880}$ and $IRPL_{955}$, which decrease due to the leakage of charge from the trap, indicating the influence of an alternative route. (2) Part of the excited state to ground state relaxation (τ_3) seems to be rather independent of the size of the trapped charge population and thus reflects the main excited state to ground state transition in $IRPL_{880}$ and $IRPL_{955}$ centres, with an average lifetime of 18-20 µs, dependent on the IRPL signal investigated. (3) Slower IRSL lifetimes (cf. Ankjærgaard et al., 2009, Ankjærgaard and Jain, 2010; Riedesel et al., 2023) represent a process different to excited state tunnelling, this could either include slower electron-hole recombination via the band-tail states (e.g. Ankjærgaard and Jain, 2010; Jain and Ankjærgaard, 2011), or alternative processes such as the release of displaced ions upon thermal or optical stimulation (e.g. Garcia-Guinea et al., 1999), which has been suggested to explain slow lifetimes measured in feldspar IRSL (Spooner et al., under review).

6 Conclusions

In this paper we performed time-resolved infrared photoluminescence (IRPL) measurements to constrain excited state lifetimes in IRPL emitting electron trapping centres in chemically and structurally different feldspars. While the data can be fitted with a three component off-time decay for the $IRPL_{880}$ and $IRPL_{955}$ signals, we only confidently discuss the two slower lifetimes (τ_2 and τ_3) because of the laser afterglow in the initial off time signal. τ_3 dominates the off-time signal in most samples, with a minimum contribution of 33 % in $IRPL_{880}$ (FSM-3) and 29 % in $IRPL_{955}$ (Al-I). τ_2 is only dominating the signal in two samples for $IRPL_{880}$ and three samples for $IRPL_{955}$, with a maximum contribution of 67 % in $IRPL_{880}$ (FSM-3) and 52 % in $IRPL_{955}$ (Al-I).

τ_3 decreases slightly with decreasing K-feldspar content. For $IRPL_{880}$ τ_3 varies between ~7 µs and ~25 µs, with most lifetimes ranging from 15 µs to 25 µs. In case of $IRPL_{955}$ τ_3 off-time lifetimes range from 8 µs to 22 µs, with the majority of measured lifetimes ranging from 15 µs to 22 µs and an average of 18-20 µs, dependent on the IRPL signal measured.

We tested the influence of thermal depletion of the trapped electron population on the lifetimes by facilitating a pulse annealing experiment. The results shows that whilst τ_2 decreases with increasing preheat temperature, τ_3 remains constant, indicating that τ_3 is independent of the trapped electron population.

Comparing IRPL lifetimes with published IRSL lifetimes reveals that at least some part of the charge leakage from the electron trapping centres to the recombination centres happens on time scales faster than excited state to ground state relaxation within the electron trap. We identify three processes governing luminescence production in feldspars (1) fast leakage of electrons from the electron traps

to the recombination centres via excited state tunnelling, (2) excited state to ground state transitions within the electron trap and (3) a slower process of either electron-hole recombination via the band-tail states or via an alternative process (e.g. ion movement).

Acknowledgements

We would like to thank Myungho Kook (DTU) for technical support during the time-resolved IRPL measurements and Anthony M.T. Bell for performing the XRF and XRD measurements. We would like to thank our colleagues who provided some of the samples used in this study: Jan-Pieter Buylaert (DTU, Denmark) for FSM-13, Geoff A.T. Duller (Aberystwyth University, United Kingdom) for FSM-6 and Adrian A. Finch (University of St. Andrews, United Kingdom) for CLBR. SR acknowledges support by the European Union's Horizon Europe research and innovation programme (RECREATE, grant no. 101103587) during writing of the manuscript.

References

Ankjærgaard, C., Jain, M., Kalchgruber, R., Lapp, T., Klein, D., McKeever, S.W.S., Murray, A.S., Morthekai, P., 2009. Further investigations into pulsed optically stimulated luminescence from feldspars using blue and green light. Radiation Measurements 44, 576-581.

Ankjærgaard, C., Jain, M., 2010. Optically stimulated phosphorescence in orthoclase feldspar over the millisecond to second time scale. Journal of Luminescence 130, 2346-2355.

Bates, D.M., DebRoy, S., 2018. nls function—nonlinear least squares. R Core Team and contributors worldwide. The R stats package version 3.5.0.

Cassadanne, J.P., Roditi, M., 1996. The location, geology and mineralogy of gem tourmalines in Brazil. Journal of Gemmology 25 (4), 263–298.

Chithambo, M.L., 2003. Dependence of the thermal influence on luminescence lifetimes from quartz on the duration of optical stimulations. Radiation Measurements 37, 167–175.

Clark, R.J., Bailiff, I.K., Tooley, M.J., 1997. A preliminary study of time-resolved luminescence in some feldspars. Radiation Measurements 27, 211–220.

Clark, R.J., Bailiff, I.K., 1998. Fast time-resolved luminescence emission spectroscopy in some feldspars. Radiation Measurements 29, 553–560.

Cunningham, G.J., 1981. Petrology and Geochemistry of Lewisian Pegmatites and Granites, N.W., Scotland. PhD thesis. Imperial Collage London, United Kingdom.

Deer, W.A., Howie, R.A., Zussman, J., 2013. An Introduction to the Rock-Forming minerals, third ed. Mineralogical Society of Great Britain and Ireland.

Demas, J.N., 1983. Excited State Lifetime Measurements. New York, London, Academic Press, 273 p.

Garcia-Guinea, J., Townsend, P.D., Sanchez-Muñoz, L., Rojo, J.M., 1999. Ultraviolet-blue ionic luminescence of alkali feldspars from bulk and interfaces. Physics and Chemistry of Minerals 26, 658-667.

Govindaraju, K., 1995. Update (1984-1995) on two GIT-IWG geochemical reference samples: albite from Italy, Al-I and iron formation sample from Greenland, IF-G. Geostandards Newsletter 19, 55–96.

Huntley, D.J., Lamothe, M., 2001. Ubiquity of anomalous fading in K-feldspars and the measurement and correction for it in optical dating. Canadian Journal of Earth Sciences 38, 1093–1106.

Hütt, G., Jaek, I., Tchonka, J., 1988. Optical Dating: K-feldspars optical response stimulation spectra. Quaternary Science Reviews 7, 381-385.

Jain, M., Ankjærgaard, C., 2011. Towards a non-fading signal in feldspar: Insight into charge transport and tunnelling from time-resolved optically stimulated luminescence. Radiation Measurements 46, 292-309. doi:10.1016/j.radmeas.2010.12.004

Jain, M., Kumar, R., Kook, M., 2020. A novel coupled RPL/OSL system to understand the dynamics of the metastable states. Scientific Reports 10, 15565. https://doi.org/10.1038/s41598-020-72434-4

Kars, R.H., Wallinga, J., Cohen, K.M., 2008. A new approach towards anomalous fading correction for feldspar IRSL dating – tests on samples in field saturation. Radiation Measurements 43, 786–790.

Kars, R.H., Poolton, N.R.J., Jain, M., Ankjærgaard, C., Dorenbos, P., Wallinga, J., 2013. On the trap depth of the IR-sensitive trap in Na- and K-feldspar. Radiation Measurements 59, 103-113. http://dx.doi.org/10.1016/j.radmeas.2013.05.002

Kook, M., Kumar, R., Murray, A.S., Thomsen, K.J., Jain, M., 2017. Instrumentation for the non-destructive optical measurement of trapped electrons in feldspar. Radiation Measurement 120, 247-252. https://doi.org/10.1016/j.radmeas.2018.06.001

Kumar, R., Kook, M., Murray, A.S., Jain, M., 2018. Towards direct measurement of electrons in metastable states in K-feldspar: Do infrared-photoluminescence and radioluminescence probe the same trap? Radiation Measurements 120, 7-13. https://doi.org/10.1016/j.radmeas.2018.06.018

Kumar, R., Kook, M., Jain, M., 2020. Understanding the metastable states in K-Na aluminosilicates using novel site-selective excitation-emission spectroscopy. Journal of Physics D: Applied Physics 53, 465301. https://doi.org/10.1088/1361-6463/aba788

Kumar, R., Kook, M., Jain, M., 2021. Sediment dating using Infrared Photoluminescence. Quaternary Geochronology 62, 101147. https://doi.org/10.1016/j.quageo.2020.101147

Lapp, T., Jain, M., Ankjærgaard, C., Pritzel, L., 2009. Development of pulsed stimulation and Photon Timer attachments to the Risø TL/OSL reader. Radiation Measurements 44, 571-575. doi:10.1016/j.radmeas.2009.01.012

Li, B., Li, S.H., 2011. Luminescence dating of K-feldspar from sediments: A protocol without anomalous fading correction. Quaternary Geochronology 6, 468-479. doi:10.1016/j.quageo.2011.05.001

Pagonis, V., Morthekai, P., Singhvi, A.K., Thomas, J., Balaram, V., Kitis, G., Chen, R., 2012. Time-resolved infrared stimulated luminescence signals in feldspars: Analysis based on exponential and stretched exponential functions. Journal of Luminescence 132, 2330-2340. https://doi.org/10.1016/j.jlumin.2012.04.020

Prasad, A.K., Poolton, N.R.J., Kook, M., Jain, M., 2017. Optical dating in a new light: A direct, non-destructive probe of trapped electrons. Scientific Reports 7: 12097. https://doi.org/10.1038/s41598-017-10174-8

Riedesel, S., King, G.E., Prasad, A.K., Kumar, R., Finch, A.A., Jain, M., 2019. Optical determination of the width of the band-tail states, and the excited and ground state energies of the principal dosimetric trap in feldspar. Radiation Measurements 125, 40-51.

Riedesel, S., 2020. Exploring variability in the luminescence properties of feldspars. PhD Thesis Aberystwyth University.

Riedesel, S., Kumar, R., Duller, G.A.T., Roberts, H.M., Bell, A.M.T., Jain, M., 2021a. Site-selective characterisation of electron trapping centres in relation to chemistry, structural state and mineral phases present in singly crystal alkali feldspars. Journal of Physics D: Applied Physics 54, 385107.

Riedesel, S., Bell, A.M.T., Duller, G.A.T., Finch, A.A., Jain, M., King, G.E., Pearce, N.J., Roberts, H.M., 2021b. Exploring sources of variation in thermoluminescence emissions and anomalous fading in alkali feldspars. Radiation Measurements 141, 106541.

Riedesel, S., Duller, G.A.T., Ankjærgaard, 2023. Time-resolved infrared stimulated luminescence of the blue and yellow-green emissions – Insights into charge recombination in chemically and structurally different alkali feldspars. Journal of Luminescence 257, 119724.

Sanderson, D.C.W., Clark, R.J., 1994. Pulsed photostimulated luminescence of alkali feldspars. Radiation Measurements 23, 633-639.

Schlag, E.W., Schneider, S., Fischer, S.F., 1971. Lifetimes in excited states. Annual Review of Physical Chemistry 22, 465-526.

Spooner, N.A., Williams, O.M., Questiaux, D.G., under review. Pulsed infrared stimulated luminescence measurements for mechanism studies in feldspars. Under review for publication in Radiation Measurements.

Thiel, C., Buylaert, J.-P., Murray, A.S, Terhorst, B., Hofer, I., Tsukamoto, S., Frechen, M., 2011. Luminescence dating oft he Stratzing loess profiel (Austria) – Testing the potential of an elevated temperature post-IR IRSL protocol. Quaternary International 234, 23-31. doi:10.1016/j.quaint.2010.05.018

Thomsen, K.J., Murray, A.S, Jain, M., Bøtter-Jensen, L., 2008. Laboratory fading rates of various luminescence signals from feldspar-rich sediment extracts. Radiation Measurements 43, 1474-1486. doi:10.1016/j.radmeas.2008.06.002

Tsukamoto, S., Denby, P.M., Murray, A.S., Bøtter-Jensen, L., 2006. Time-resolved luminescence from feldspars: new insights into fading., Radiation Measurements 41, 790–795.

Ussher, W.A.E., Barrow, G., McAlister, D.A., 1909. The Geology of the Country Around Bodmin and St. Austell. Memoirs of the Geological Survey England and Wales – Explanation of Sheet 347.

Visocekas, R., 1985. Tunnelling radiative recombination on labradorite: its association with anomalous fading of thermoluminescence. Nuclear Tracks and Radiation Measurements 10, 521–529.

Wintle, A.G., 1973. Anomalous fading of thermoluminescence in mineral samples. Nature 245, 143–144.

Supplementary Material

Svenja Riedesel[a] and Mayank Jain[b]

[a]Radiation Physics Division, Department of Physics, Technical University of Denmark, Risø Campus, Rosklide, Denmark

[b]Institute of Geography, University of Cologne, Cologne, Germany

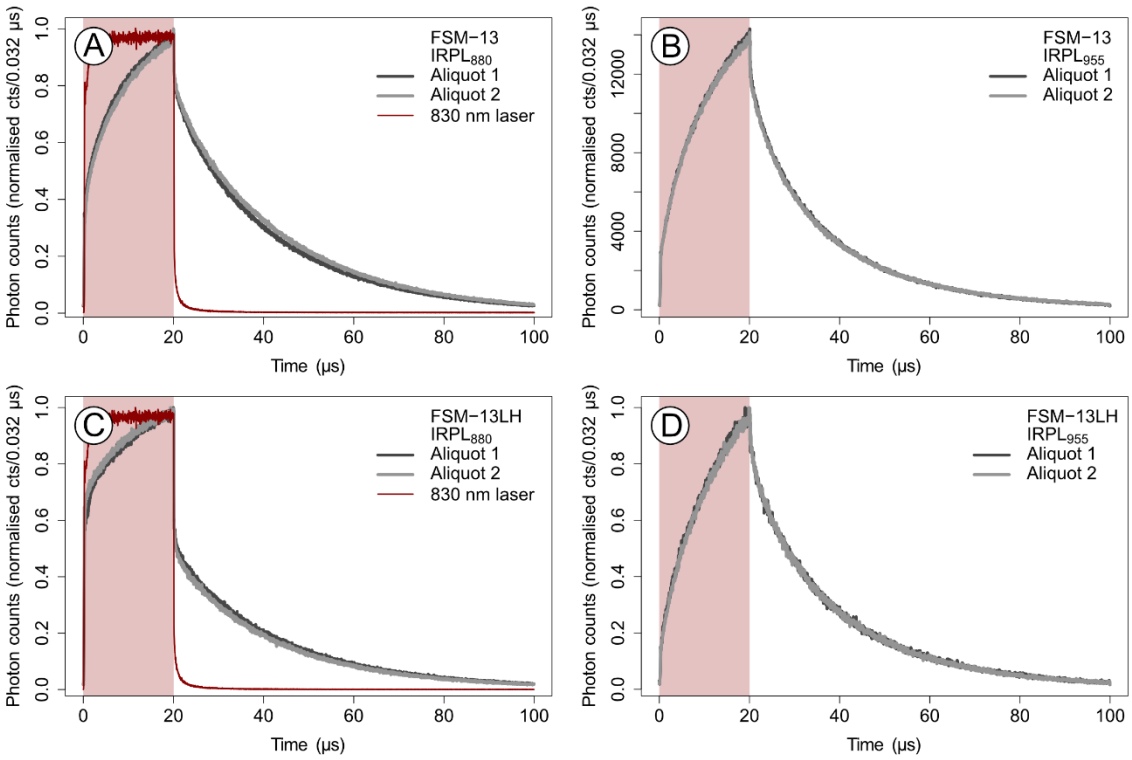

Fig. S1. A) Time-resolved $IRPL_{880}$ signal of single-phase microcline sample FSM-13, B) time resolved $IRPL_{955}$ of single-phase microcline sample FSM-13, C) time-resolved $IRPL_{880}$ signal of artificially disordered sample FSM-13LH, D) time-resolved $IRPL_{955}$ signal of artificially disordered sample FSM-13LH. The on-time is highlighted with the shaded rectangle.

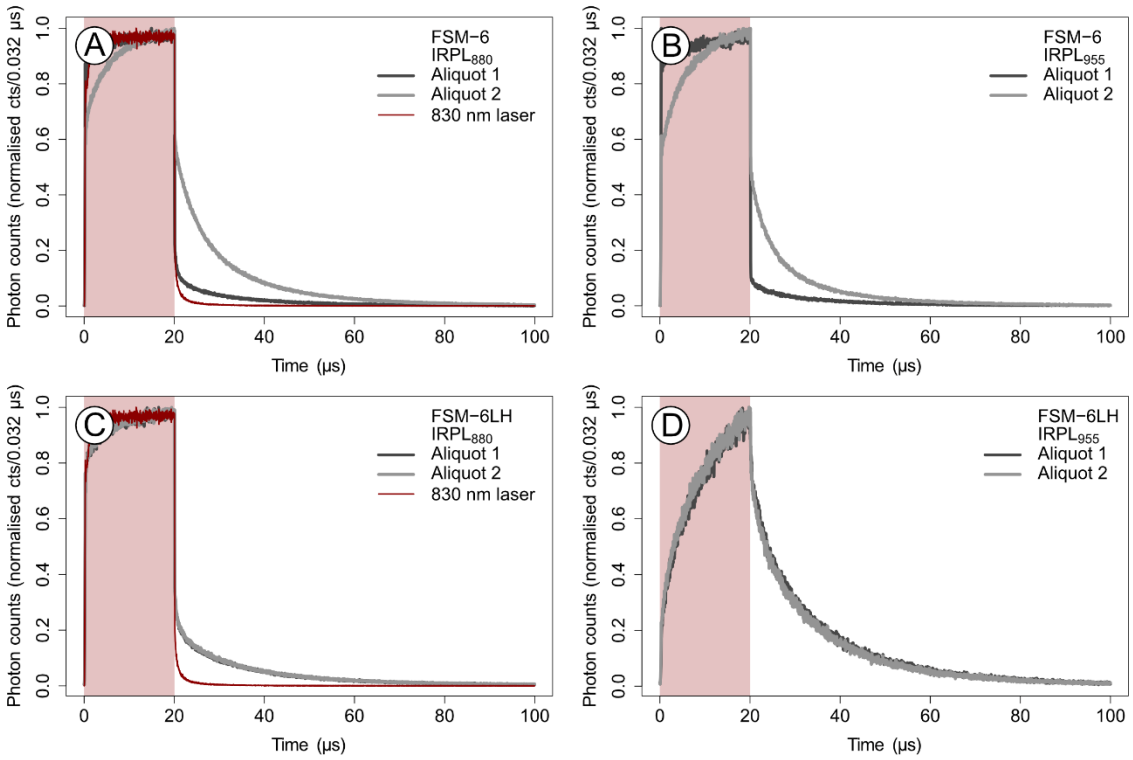

Fig. S2. A) Time-resolved $IRPL_{880}$ signal of perthite FSM-6, B) time resolved $IRPL_{955}$ of perthite FSM-6, C) time-resolved $IRPL_{880}$ signal of artificially disordered sample FSM-6LH, D) time-resolved $IRPL_{955}$ signal of artificially disordered sample FSM-6LH. The on-time is highlighted with the shaded rectangle.

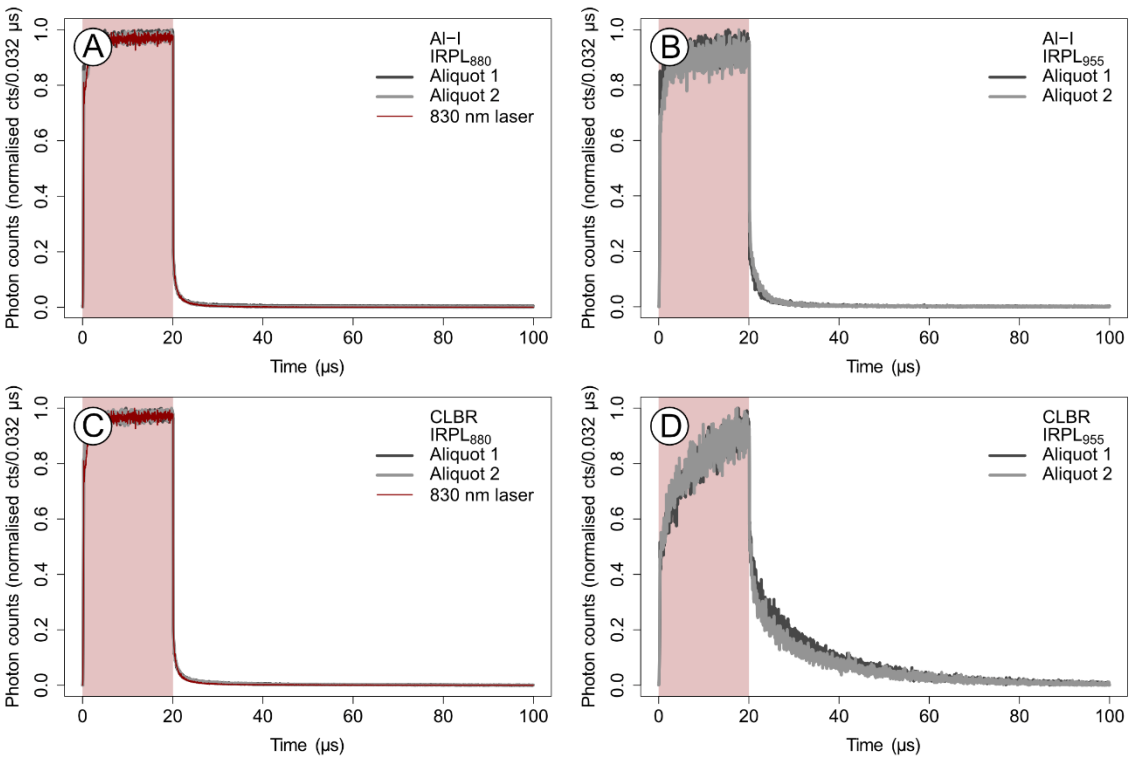

Fig. S3. Time-resolved $IRPL_{880}$ signal of single-phase samples Al-I (A) and CLBR (C), time resolved $IRPL_{955}$ of single-phase samples Al-I (B) and CLBR (D). The on-time is highlighted with the shaded rectangle.

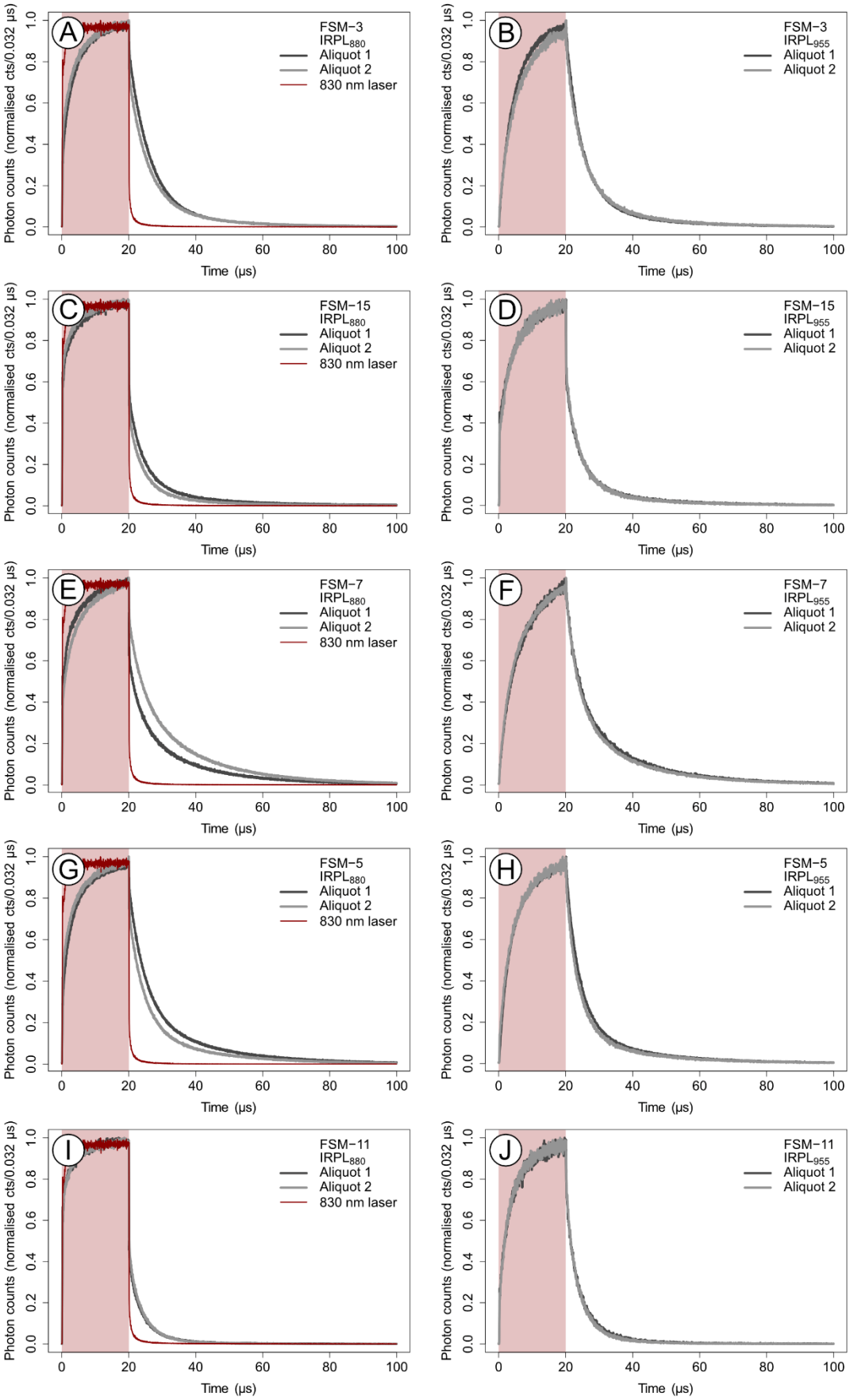

Fig. S4. Time-resolved $IRPL_{880}$ and $IRPL_{955}$ signals, respectively, for perthitic samplesFSM-3 (A and B), FSM-15 (C and D), FSM-7 (E and F), FSM-5 (G and H) and FSM-11 (I and J).

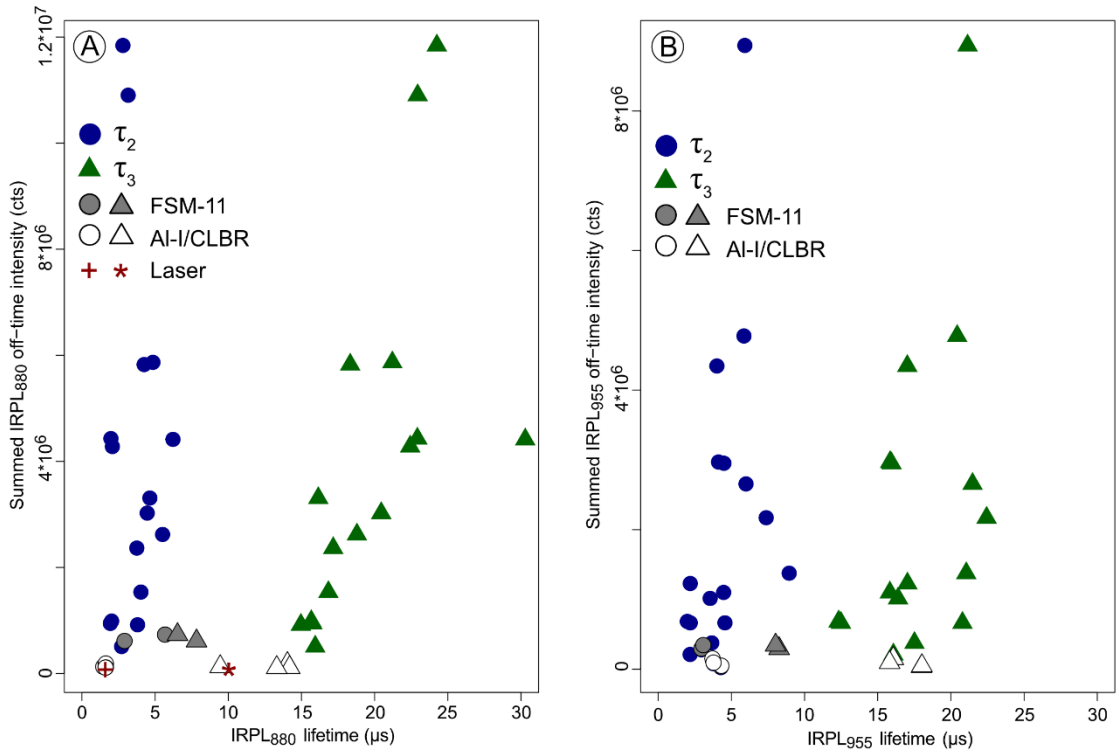

Fig. S5. A) IRPL880 intensity compared to the fitted lifetimes. B) IRPL955 intensity compared to the fitted lifetimes. The signal and lifetime of the laser off-time signal measured on an empty cup is display as a comparison.

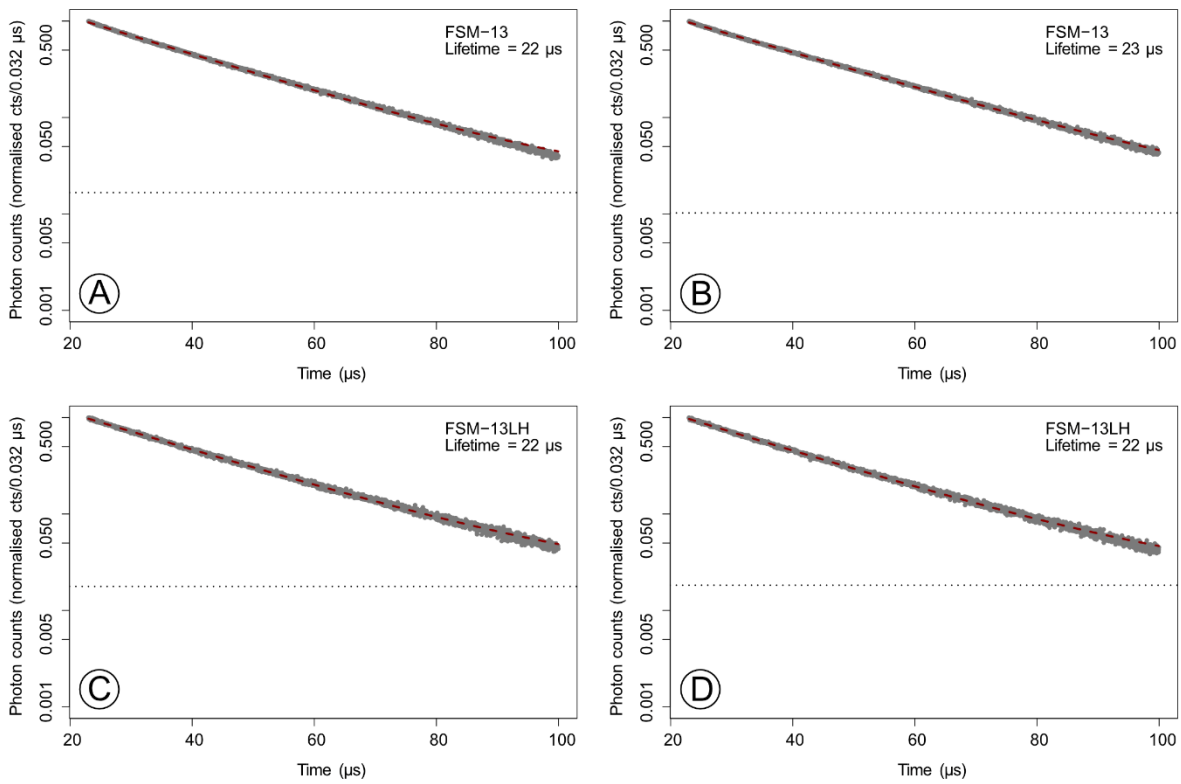

Fig. S6. $IRPL_{880}$ off-time signal excluding the initial 3 µs fitted using a single exponential function to enable a comparison with the data published by Kumar et al. (2020). The data is displayed for two aliquots of samples FSM-13 (A, B) and FSM-13LH (C, D).

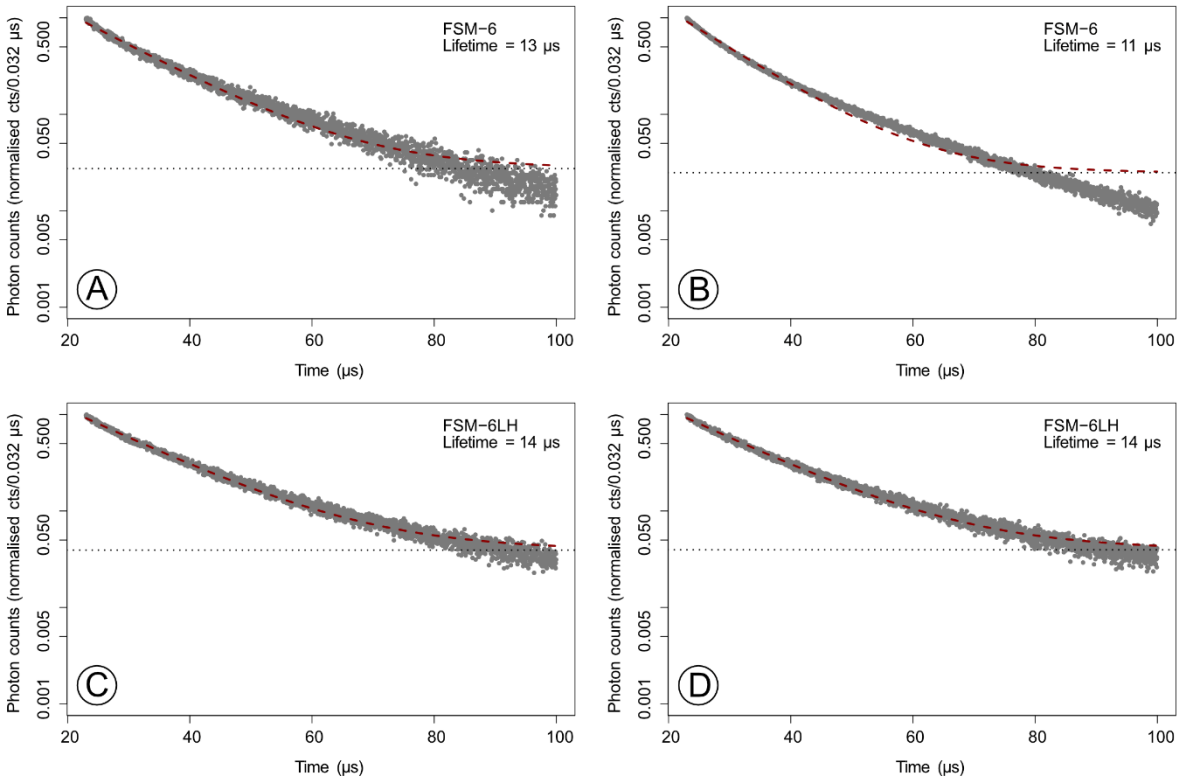

Fig. S7. $IRPL_{880}$ off-time signal excluding the initial 3 µs fitted using a single exponential function to enable a comparison with the data published by Kumar et al. (2020). The data is displayed for two aliquots of samples FSM-6 (A, B) and FSM-6LH (C, D).

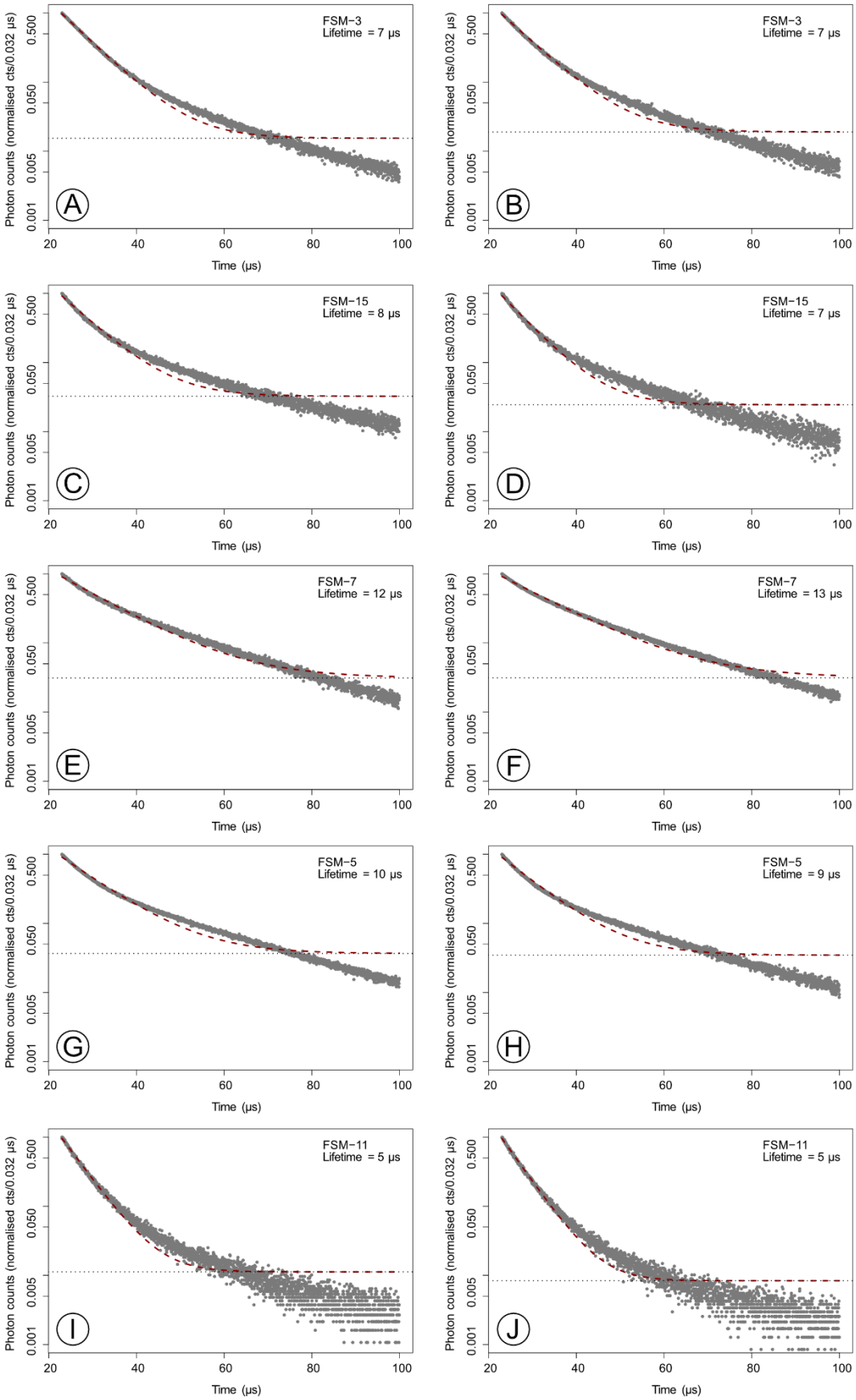

Fig. S8. IRPL$_{880}$ off-time signal excluding the initial 3 µs fitted using a single exponential function to enable a comparison with the data published by Kumar et al. (2020). The data is displayed for two aliquots of perthitic samples FSM-3 (A, B), FSM-15 (C, D), FSM-7 (E, F), FSM-5 (G, H) and FSM-11 (I, J).

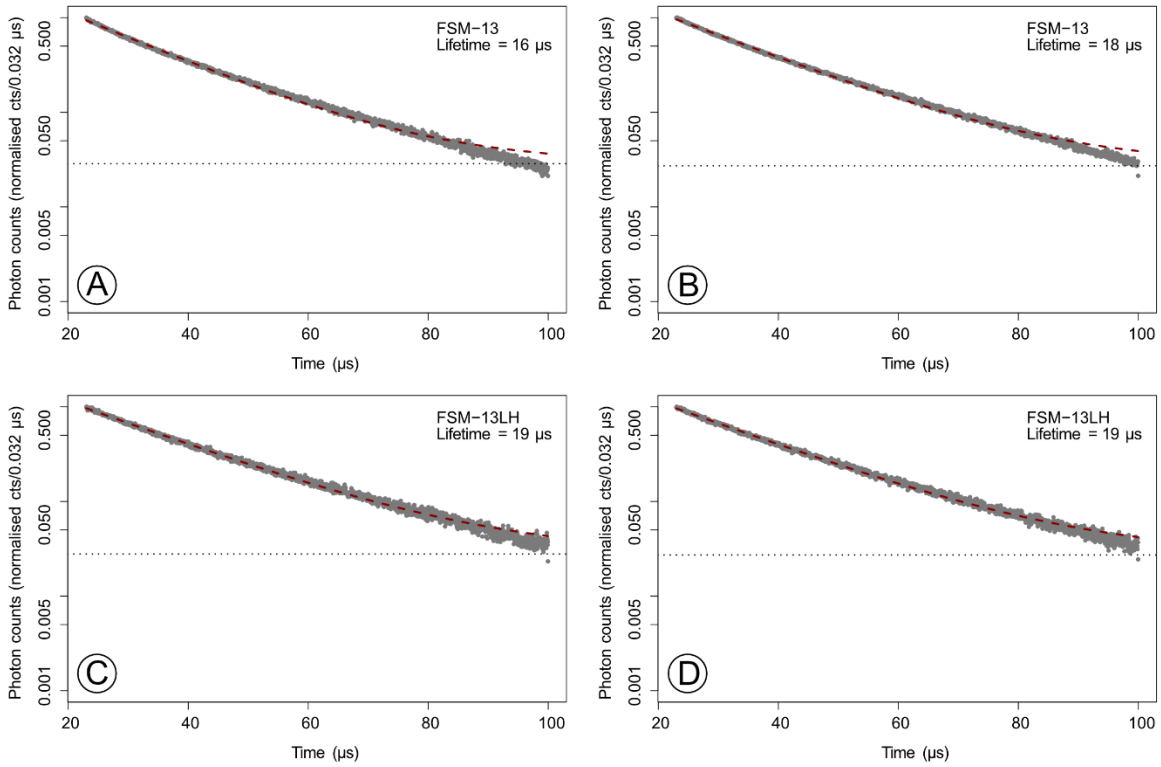

Fig. S9. IRPL$_{955}$ off-time signal excluding the initial 3 µs fitted using a single exponential function to enable a comparison with the data published by Kumar et al. (2020). The data is displayed for two aliquots of samples FSM-13 (A, B) and FSM-13LH (C, D).

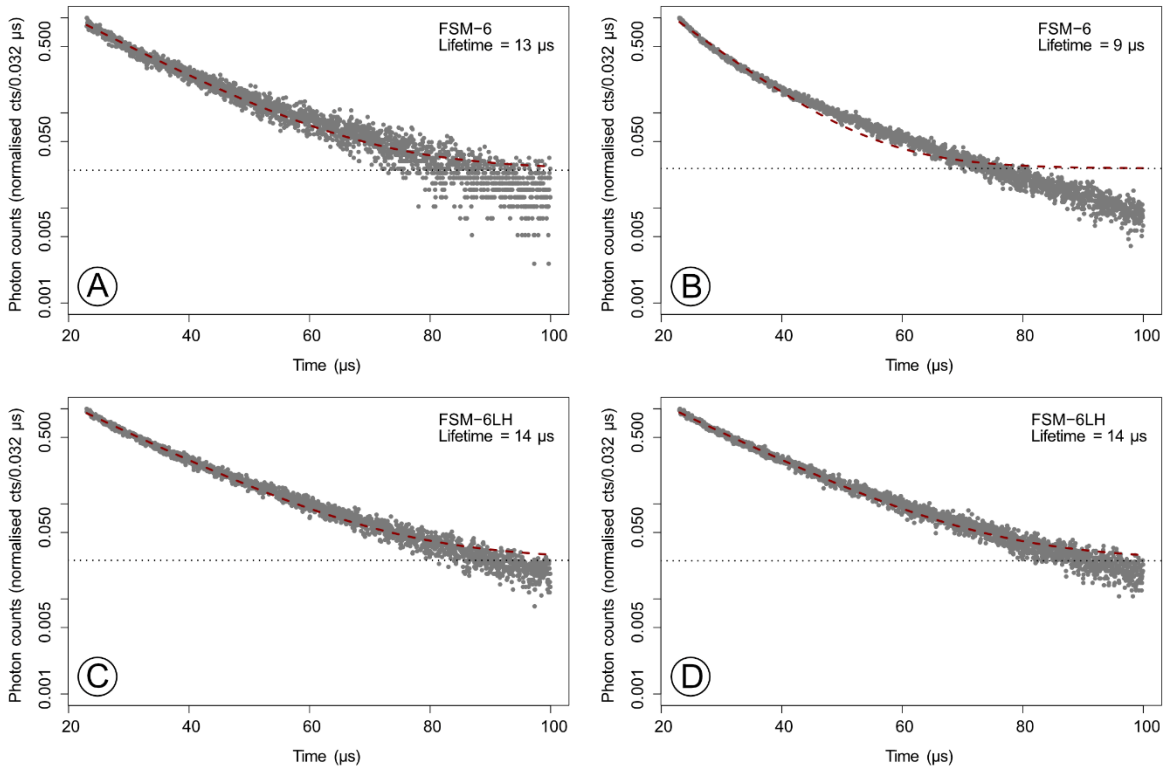

Fig. S10. IRPL$_{955}$ off-time signal excluding the initial 3 µs fitted using a single exponential function to enable a comparison with the data published by Kumar et al. (2020). The data is displayed for two aliquots of samples FSM-6 (A, B) and FSM-6LH (C, D).

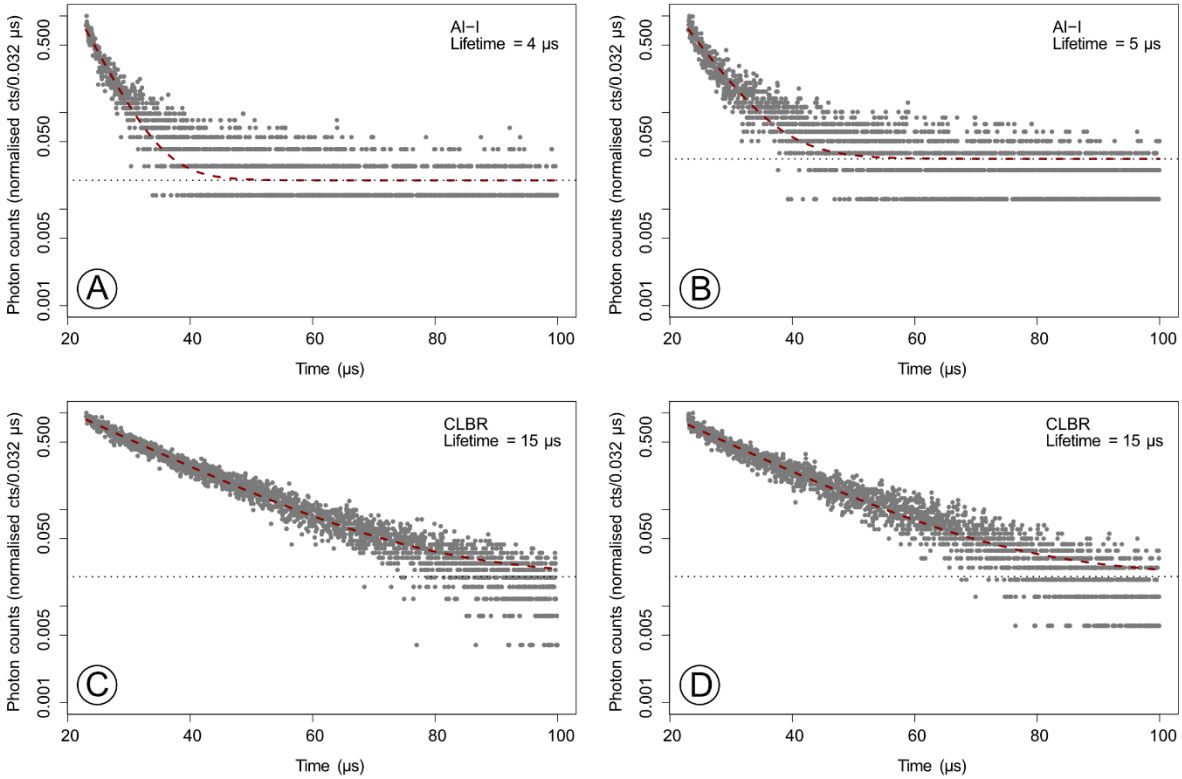

Fig. S11. IRPL$_{955}$ off-time signal excluding the initial 3 µs fitted using a single exponential function to enable a comparison with the data published by Kumar et al. (2020). The data is displayed for two aliquots of samples Al-I (A, B) and CLBR (C, D).

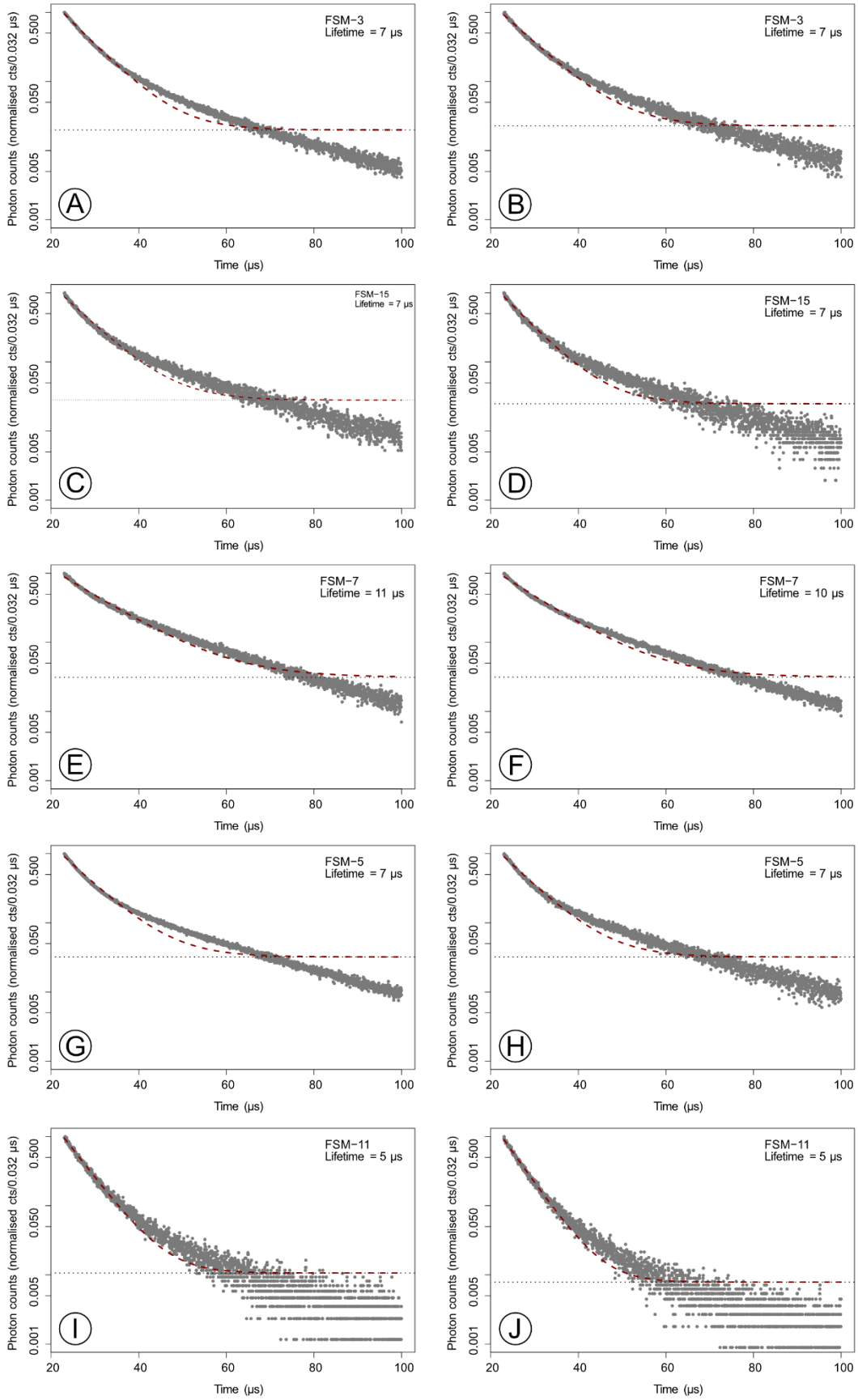

Fig. S12. $IRPL_{955}$ off-time signal excluding the initial 3 μs fitted using a single exponential function to enable a comparison with the data published by Kumar et al. (2020). The data is displayed for two aliquots of perthitic samples FSM-3 (A, B), FSM-15 (C, D), FSM-7 (E, F), FSM-5 (G, H) and FSM-11 (I, J).